Title	Crystal structure of peroxisomal targeting signal-2 bound to its receptor complex Pex7p–Pex21p
Author(s)	Pan, Dongqing; Nakatsu, Toru; Kato, Hiroaki
Citation	Nature Structural & Molecular Biology (2013)
Issue Date	2013-06-30
URL	http://hdl.handle.net/2433/175497
Right	© 2013 Nature Publishing Group, a division of Macmillan Publishers Limited. All Rights Reserved.; 2013-12-30 .
Type	Journal Article
Textversion	author

Crystal structure of peroxisomal targeting signal–2 bound to its receptor complex

Pex7p–Pex21p

Dongqing Pan[1], Toru Nakatsu[1,2], and Hiroaki Kato[1,2]

[1]Department of Structural Biology, Graduate School of Pharmaceutical Sciences, Kyoto

University, 46-29 Yoshida-Shimoadachi, Sakyo-ku, Kyoto 606-8501, Japan.

[2]RIKEN SPring-8 Center, 1-1-1, Kouto, Sayo, Hyogo 679-5148, Japan.

Correspondence should be addressed to Dongqing Pan (pan.dongqing@pharm.kyoto-u.ac.jp)

or Hiroaki Kato (katohiro@pharm.kyoto-u.ac.jp).

Running title: Structural basis for PTS2 recognition

Abstract

Appropriate targeting of matrix proteins to peroxisomes is mainly directed by two types of

peroxisomal targeting signals, PTS1 and PTS2. Although the basis of PTS1 recognition has

been revealed by structural studies, that of PTS2 recognition remains elusive. Here, we present

the crystal structure of a hetero-trimeric PTS2-recognition complex from *Saccharomyces

cerevisiae*, containing Pex7p, the C-terminal region of Pex21p, and the PTS2 of the

peroxisomal 3-ketoacyl-CoA thiolase. Pex7p forms a beta-propeller structure and provides a

platform for cooperative interactions with both the amphipathic PTS2 helix and Pex21p. The

C-terminal region of Pex21p directly covers the hydrophobic surfaces of both Pex7p and PTS2,

and the resulting hydrophobic core is the primary determinant of stable complex formation.

Together with *in vivo* and *in vitro* functional assays of Pex7p and Pex21p variants, our findings

reveal the molecular mechanism of PTS2 recognition.

INTRODUCTION

Many proteins use targeting signals to reach the appropriate organelles. Organelle-specific

receptor proteins recognize these targeting signals by direct protein-protein interactions. This is

also the case with peroxisomes, single membrane-bound organelles containing enzymes

involved in various metabolic pathways such as hydrogen peroxide detoxification and

β-oxidation of fatty acids[1]. More than twenty proteins work in concert to assemble functional

peroxisomes. These proteins are named peroxins, and are encoded by the *PEX* genes[2,3]. In

human, defects in peroxins disrupt import of essential enzymes into peroxisomes, resulting in a

group of human diseases known as the peroxisomal biogenesis disorders (PBDs)[4]. The receptor

proteins that recognize peroxisomal targeting signals are crucial peroxins.

There are two types of targeting signals for peroxisomal matrix proteins: peroxisomal

targeting signal–1 (PTS1) at C-termini, and peroxisomal targeting signal–2 (PTS2) near

N-termini[2]. PTS1 is recognized by the peroxin Pex5p, and PTS2 is recognized by the peroxin

Pex7p together with a co-receptor peroxin. Crystal structures of the PTS1-binding domain of

Pex5p have been solved in apo-form[5], with a PTS1 peptide[6] or with a PTS1-cargo (mSCP2)[5].

On the other hand, no crystal structure of Pex7p or the PTS2-interaction domain of the

co-receptor peroxin, ligated with or without PTS2, has been reported to date; consequently,

many questions remain unsolved[7,8].

One important question regards what interactions between PTS2 and the receptors determine the characteristic sequence motif of PTS2. The PTS2 sequence was initially identified in rat peroxisomal thiolase[9,10]. Later, the sequence motif of PTS2 was refined to R-[L/V/I/Q]-xx-[L/V/I/H]-[L/S/G/A]-x-[H/Q]-[L/A] (x = any residue) by bioinformatics analysis of available functional PTS2 sequences[11]. Positions 2, 5, and 9 of this motif are mostly limited to hydrophobic residues whereas positions 1 and 8 are limited to hydrophilic residues. In order to explain these sequence constraints, the detailed interactions between PTS2 and its receptors must be determined.

Another question regards how Pex7p provides the binding site for PTS2. Pex7p is an evolutionarily conserved soluble protein containing six WD40 repeats[12-20]. The first Pex7p identified was *S. cerevisiae* Pex7p (also known as Peb1p or Pas7p), which was shown to be the receptor of Fox3p (also known as Pot1p)[12,13,21]. Fox3p contains a functional PTS2 at its N-terminus[21,22] and functions as a 3-ketoacyl-CoA thiolase (EC 2.3.1.16) at the final step of the β-oxidation[1]. Human Pex7p was identified as the homolog of *S. cerevisiae* Pex7p and linked to a fatal PBD, rhizomelic chondrodysplasia punctata type 1 (RCDP1)[14-16,23,24]. Since Pex7p is a WD40 protein, its structure has been modeled using the structures of other WD40 proteins, and

the possible interactions between Pex7p and PTS2 has been proposed[25]. However, we still lack

a complete view of the interactions between Pex7p and PTS2.

A more challenging, but also intriguing, question regards how the co-receptor peroxin

assists Pex7p in PTS2 recognition. The co-receptor peroxin is species-specific. Paralogous

peroxins, Pex18p and Pex21p, act as the co-receptor of Pex7p in *S. cerevisiae*[26], and their

homolog Pex20p exists in other fungi[20,27,28]. The PTS1 receptor, Pex5p, also acts as the

co-receptor of Pex7p in *Arabidopsis thaliana*[19,29] and in mammals[30-32]. The domain structures

of these co-receptor peroxins share common features: First, their N-terminal domains contain a

conserved motif[27,33] that is ubiquitinated during the recycling of receptors from peroxisomal

membrane to cytosol[34,35]. Second, the Pex14p-binding motif (Wxxx[F/Y]) interacts with

Pex14p[36], a peroxin that forms a docking complex on the peroxisomal membrane. Third, the

Pex7p-binding domain (Pex7pBD) is essential for the interaction with Pex7p and the import of

PTS2-cargos into peroxisomes[27,32,33]. In Pex18p, Pex21p, and Pex20p, Pex7pBD resides close

to the C-termini, whereas in Pex5p, an additional PTS1-binding domain flanks the C-terminal

side of Pex7pBD[27]. Pex7pBD seems to be the most important region for interaction with Pex7p,

but where does Pex7pBD bind on Pex7p, and how does it support PTS2-cargo transport?

Since their discoveries, PTS2, Pex7p, and the co-receptor peroxins have been studied and

characterized. However, the details of the interactions among the three factors remain unclear.

To understand the mechanism of PTS2 recognition and the molecular basis of RCDP1, we solved the crystal structure of a PTS2-recognition complex from *S. cerevisiae*. The structure contains Pex7p, the C-terminal region of Pex21p (Lys190–Asp288; hereafter referred to as Pex21pC), and the N-terminal 15 residues of Fox3p (hereafter referred to as Fox3pN), and reveals the conserved mechanism of PTS2 recognition and its differences with other N-terminal targeting signals.

RESULTS

Preparation of Pex7p–Pex21pC–Fox3pN-MBP complex

We purified the ternary complex containing Pex7p, Pex21pC, and Fox3pN-MBP by mixing the three proteins after purification of individual components. Pex7p, which was difficult to obtain in soluble form using an *Escherichia coli* expression system, was expressed in *Pichia pastoris* as GST-fusion protein. Well-diffracting plate crystals grew when a Pex7p mutant with a nine-residue deletion (Δ257–265) was used instead of wild-type Pex7p (Fig. 1, Supplementary Fig. 1). Pex21pC was sufficient to form the ternary complex and was more resistant to degradation than the homologous region of Pex18p; it was therefore chosen for crystallization. Fox3pN-MBP, used instead of full-length Fox3p, was constructed by attaching Fox3pN to the N-terminus of the maltose-binding protein (MBP) from *E. coli* by a two-residue linker (Arg-Ser) (Fig. 1a).

Pex7p, Pex21pC, and Fox3p exhibited cooperative complex formation, as demonstrated by pull-down experiments using wild-type Pex7p (or GST-Pex7p), Pex21pC (or MBP-Pex21pC), and Fox3p (Fig. 2). The ternary complex containing Pex7p, Pex21pC, and Fox3p was much more stable than any of the binary complexes. Although we did not detect the

binary interaction of Fox3p with Pex7p in the buffer with 300 mM NaCl by the pull-down experiment, we observed weak but specific binding of Fox3p to Pex7p in the buffer with 50 mM NaCl (Supplementary Fig. 2).

Overall structure of the hetero-trimeric complex

The hetero-trimeric structure of Pex7p–Pex21pC–Fox3pN-MBP was solved by molecular replacement using crystal structures of MBP and WDR5 as search models. The overall electron-density map was clear (Supplementary Fig. 3), allowing us to construct atomic models for all regions of Pex7p, Pex21pC, and Fox3pN-MBP except for the disordered loops of Pex7p (DL1, Lys164–Arg174; DL2, Leu253–Ser272; DL3, Asp317–Tyr323) and Pex21pC (DL1, Lys190–Gln196; DL2, Pro212–Leu223; DL3, Lys252–Ala259) (Fig. 1c, Supplementary Fig. 1a,b). Only one hetero-trimer exists in the crystallographic asymmetric unit, and the model was refined at 1.8 Å resolution to a free *R*-factor of 22.4% (Table 1).

The resulting structure revealed the characteristic assembly of the three proteins (Fig. 1b,c). Pex7p forms a ring structure with a seven-bladed β-propeller fold. Pex21pC consists of three parts: a cluster of three α-helices (α1–3), a small three-stranded β-sheet (β1–3), and a stretched C-terminal loop. The helical cluster and the β-sheet of Pex21pC bind on the rim of the

top surface of Pex7p, and they cooperatively form a binding pocket for Fox3pN. The

C-terminal loop of Pex21pC extends along the side of Pex7p and does not interact with Fox3pN.

Fox3pN adopts an α-helical conformation and stretches from the globular region of MBP into

the binding pocket prepared by Pex7p and Pex21pC. The buried surface area of Fox3pN (1,240

$Å^2$) in the pocket accounts for more than 70% of its total solvent-accessible surface area (1,740

$Å^2$).

Special motif of Pex7p and Pex7p–Pex21p complex formation

The crystal structure revealed structural features important for Pex7p–Pex21p complex

formation. Although the framework of Pex7p is the same as that of typical WD40 proteins[37], it

contains a special region at its N-terminus. The N-terminal 44 residues of Pex7p have low

sequence similarity to other WD40 motifs[13], but this region can nonetheless assume a

WD40-like fold and complete the ring structure (Fig. 1c, Supplementary Fig. 4ab). In this

N-terminal region, the loop between β-strand 1B and 1C (Asn31–Asn37) is longer than other

adjacent loops composing the top surface of Pex7p, and thus forms a bulge (Fig. 1c, 3a,

Supplementary Fig. 4a), hereafter referred as to the bulge loop. The bulge loop contains a

six-residue consensus motif, [N/H]-[F/Y]-G-[L/I]-[V/L/I/S/A]-G, whose length and

composition are conserved in Pex7p homologs (Supplementary Fig. 1a). By partially adopting

a 3_{10}-helix structure, the bulge loop exposes the hydrophobic residues Phe32, Leu34, and Val35

on its surface (Fig. 3b). When Pex7p forms a complex with Pex21pC, this protruding

hydrophobic bulge loop is covered by the hydrophobic pocket of Pex21pC formed at the hinge

region between α3 and β1 (Fig. 3b).

The bulge loop constitutes half of a hydrophobic ridge on the top surface of Pex7p (Fig.

3a) that consists of residues from blade 1 (the bulge loop), blade 6 (Leu284, Tyr304, Met306),

and blade 7 (Phe344, Trp364) (Supplementary Fig. 4a). The hydrophobic ridge contacts the

hydrophobic surface of Pex21p, which contains nine hydrophobic residues: Cys210 on α1;

Val227 and Leu231 on α2; Phe236, Ile237, Leu239, and Met240 on α3; Leu250 on β1; and

Leu262 on β2 (Fig. 3b, Supplementary Fig. 4c). Four residues of Pex7p, Phe32, Leu34, Phe344,

and Trp364, surround Pex21p Phe236 (Fig. 3b, Supplementary Fig. 3b), which is highly

conserved among the co-receptor peroxins (Supplementary Fig. 1bc).

Pex7p has another characteristic region involved in binding with Pex21pC. An acidic

patch is formed at the side of the hydrophobic ridge on blades 6 and 7 (Fig. 3a). This acidic

patch consists of two components: the side chain of Pex7p Glu343 and the clustered main-chain

C=O groups of Pex7p Met306, Thr339, and His341 (Fig. 3a, Supplementary Fig. 4a). The side

chain of Pex7p Glu343 interacts electrostatically with the side-chain OH group of Pex21p

Ser234 and the main-chain NH group of Pex21p Lys235 (Fig. 3b). Because Pex21p Ser234 and

Lys235 are located in the N-terminal portion of α3, they are positively charged by the dipole

effect of the α-helix. The clustered main-chain C=O groups of Pex7p Met306, Thr339, and

His341 are in range to form hydrogen bonds with Pex21p Lys230 (Fig. 3b).

Most of the residues forming the hydrophobic and electrostatic interfaces between Pex7p

and Pex21pC are conserved among the corresponding homologs (Supplementary Fig. 1).

PTS2 recognition by cooperation of Pex7p and Pex21p

The α-helix of Fox3pN is amphipathic. Fox3p Met1, Leu5, Ile8, Leu12, and Val13 form

the hydrophobic surface, whereas the remaining residues form the hydrophilic surface (Fig. 4a).

As a result, the key residues of PTS2 are separated in two groups: the hydrophilic key residues

(Fox3p Arg4, His11) and the hydrophobic key residues (Fox3p Leu5, Ile8, Leu12).

The binding site of PTS2 is a large cleft that holds the α-helix of Fox3pN and contains two

minor grooves that accept side chains protruding from the α-helix (Fig. 1c, 4bc). One groove is

hydrophilic and the other is hydrophobic. The hydrophilic groove at the center of the top

surface of Pex7p contains two pockets that accept the hydrophilic key residues of PTS2 (Fox3p

Arg4 and His11) (Fig. 3a, 4c). Fox3p Arg4 is surrounded by the residues of Pex7p blades 1–3, and its guanidine group is fixed by formation of salt bridges with the carboxyl groups of two acidic residues, Pex7p Asp61 and Glu106 (Fig. 3a, 4b). Fox3p His11 is surrounded by the residues of Pex7p blades 4–6, and its imidazole ring is fixed by formation of hydrogen bonds with Pex7p Tyr178, Glu222, and Tyr304. When Fox3p Arg4 and His11 bind to the top surface of Pex7p in the correct orientation, the hydrophobic residues of Fox3pN consequently fit into the hydrophobic groove (Fig. 4c), which is formed in between the hydrophobic interfaces of Pex7p and Pex21pC (Fig. 3a). All three hydrophobic key residues (Fox3p Leu5, Ile8, Leu12) of PTS2 are hidden inside the hydrophobic groove and form van der Waals contacts with Pex21p Phe236 (Fig. 4bc, Supplementary Fig. 3b). Additionally, Fox3p Met1 is embedded in the site above the bulge loop (Fig. 3a, 4bc).

Insertion of the hydrophobic side chains of PTS2 to the hydrophobic groove completes a hydrophobic core around the central residue, Pex21p Phe236 (Fig. 4b). Other components of the hydrophobic core are the hydrophobic residues that form the hydrophobic interfaces of Pex7p and Pex21p described above (Fig. 3b).

The residues of Pex7p and Pex21pC that form the binding site for PTS2 are well conserved among the corresponding homologs (Supplementary Fig. 1). In particular, the α1

helix of Pex21pC, which forms a lid to cover PTS2, is also a conserved region among the

co-receptor peroxins as with Pex21p α2 and α3, which compose Pex7pBD[8] (Supplementary Fig.

1b).

In vitro and in vivo assays of Pex7p and Pex21p mutants

To examine the functional importance of the interaction modules of Pex21p and Pex7p in

ternary complex formation and PTS2-cargo transport, we performed *in vitro* and *in vivo*

functional assays. For the *in vitro* assays, we conducted pull-down experiments using amylose

resin with purified MBP-Pex21pC (or its variants), Pex7p (or its variants), and Fox3p (Fig. 5ab).

For the *in vivo* assays, *S. cerevisiae* gene deletion strains of Pex7p alone (*Δpex7*) or both

Pex18p and Pex21p (*Δpex18Δpex21*) were created from wild-type strain BY20134 (W303-1A

background). C-terminally His₆-tagged Pex7p, Pex21p, and their variants were expressed in the

deletion strains, and the growth of these derivative strains on oleic-acid medium (SCOT agar

plate) was examined. As reported previously[13,26], *Δpex7* and *Δpex18Δpex21* exhibited growth

defects on SCOT plates due to the inability to import sufficient Fox3p into peroxisomes,

whereas *Δpex7* expressing wild-type Pex7p and *Δpex18Δpex21* expressing Pex21p exhibited

normal growth (Fig. 5c). Simultaneously, Fox3pN-EGFP and mCherry-PTS1 (PTS1 =

Ser-Lys-Leu) were co-expressed in all strains, and their localizations were observed using a confocal microscope (Supplementary Fig. 5a). Expressed Pex7p and Pex21p variants were detected by western blotting (Supplementary Fig. 5b).

To investigate the importance of the hydrophobic core, we replaced the central residue Pex21p Phe236 and the adjacent conserved residues (Pex7p Phe32, Leu34, Phe344, and Trp364) with Ala or Asp. Single-Ala mutants of these residues did not have significant effects on formation of the ternary complex (Fig. 5b). However, when we mutated Pex21p Phe236 or Pex7p Leu34 to Asp (Pex21p F236D, Pex7p L34D), or simultaneously mutated two nearby residues of Pex7p to Ala (Pex7p F32A L34A, F344A W364A), these mutants exhibited clear defects in complex formation (Fig. 5a,b). These mutants also failed to restore growth of *Δpex7* or *Δpex18Δpex21* on SCOT plates (Fig. 5c) and were unable to restore localization of Fox3pN-EGFP to peroxisomes (Supplementary Fig. 5a). Among the single-Ala mutants, the Pex7p L34A and F344A mutants were both able to import enough amount of Fox3p into peroxisomes to restore growth of *Δpex7* on SCOT plates (Fig. 5c), but the efficiency of Fox3pN-EGFP transport was not sufficient for formation of clear spots (Supplementary Fig. 5a). The Pex21p F236A mutant was less able to restore growth of *Δpex18Δpex21* on SCOT plates (Fig. 5c), although we did not observe a clear effect of this mutant on complex formation (Fig.

5a). Pex21p Ile206, located on the α1 helix, is also a component of the hydrophobic core. The Pex21p I206D mutant exhibited lower affinity for Pex7p and Fox3p (Fig. 5a) and was unable to restore growth of *Δpex18Δpex21* on SCOT plates (Fig. 5c). The results of Pex21p I206D were similar to those of the Pex21p Δα1 mutant (Δ197–211) (Fig. 5a,c). Mutations of residues outside the hydrophobic core (Pex21p I202D, K230E) did not affect complex formation (Fig. 5a), and these mutants were able to restore growth of *Δpex18Δpex21* on SCOT plates (Fig. 5c). Two Pex21p deletion mutants, ΔL (Δ214–229) and ΔC (Δ247–288), were able to restore growth of *Δpex18Δpex21* on SCOT plates (Fig. 5c). However, the deletion of the 42 C-terminal residues of the Pex21p ΔC decreased the affinity of Pex21pC for Pex7p and Fox3p (Fig. 5a).

We next examined the role of Pex7p residues that form electrostatic interactions with the hydrophilic key residues of PTS2 (Fox3p Arg4, His11). Consequently, we generated two gain-of-function variants of Pex7p that can recognize two artificial PTS2s containing Glu in place of either Arg4 or His11 in Fox3p. The mutated Pex7p containing D61R E106H lost the ability to import wild-type Fox3p into peroxisomes and failed to restore the growth of *Δpex7* on SCOT plate (Fig. 5c). When we co-expressed the Pex7p D61R E106H mutant with the Fox3p R4E mutant, the transformant was able to grow on SCOT plate as rapidly as a strain expressing wild-type Pex7p (Fig. 5c). The same result was obtained in the case of a strain co-expressing

the Pex7p Y178R Y304R and Fox3p H11E mutants. To exclude the possibility that the

restoration of growth was due to overexpression of Fox3p mutants, we co-expressed the mutant

proteins in the other combination. Neither the co-expression of Pex7p D61R E106H with

Fox3p H11E nor co-expression of Pex7p Y178R Y304R with Fox3p R4E restored growth of

Δpex7 on SCOT plates (Fig. 5c).

DISCUSSION

The crystal structure we report here reveals the spatial organization of the Pex7p–Pex21pC–Fox3pN complex and provides an explanation for the cooperative binding among Pex7p, Pex21pC, and Fox3p observed in the pull-down experiments. Both Fox3pN and Pex21pC bind to the top surface of Pex7p, which is a common interaction site for WD40 proteins[38,39]. On this surface, the hydrophobic residues of Pex7p, Pex21pC and Fox3pN cooperatively form a hydrophobic core around the central residue Pex21p Phe236. These hydrophobic residues are evolutionarily well conserved, which suggests that formation of the hydrophobic core is important for stabilizing the ternary complex. Any combination of the binary complexes (Pex7p–Fox3pN, Pex7p–Pex21pC, or Pex21pC–Fox3pN) leaves a part of the hydrophobic surface exposed to solution, destabilizing the binary complex. The electrostatic interactions between Pex7p and Pex21pC and between Pex7p and Fox3pN take place at both sides of the hydrophobic core, thus strengthening the hydrophobic effect and further stabilizing the ternary complex.

We confirmed the importance of the hydrophobic core on complex formation and PTS2-cargo transport by mutational analyses of residues inside and outside the hydrophobic core. Mutations of Pex21p Phe236 (F236A and F236D) were the most severe among the Ala

and Asp mutants examined. The effects of Asp mutations decreased as residues contributed less to the rigidity of the hydrophobic core, in the following order (i.e., from greatest to lowest effect): Pex21p F236D, Pex7p L34D, Pex21p I206D, and Pex21p I202D. We assume that a minimal threshold of rigidity of the hydrophobic core is required for functional PTS2-cargo transport. Although some of the mutants (Pex7p F344A W364A, Pex21p I206D, and Pex21p Δα1) exhibited only moderate defects in complex formation, they were unable to form hydrophobic cores with rigidities above this threshold. The decrease in affinity of the Pex21p ΔC mutant for Pex7p and Fox3p implies that the 42 C-terminal residues of Pex21p also contribute to complex formation; however, these residues are not essential for the hydrophobic-core formation or PTS2-cargo transport. Assuming that the hydrophobic core is the primary determinant of stable complex formation, destabilization of the hydrophobic core is predicted to result in PTS2-cargo release. Further studies of kinetics and thermodynamic analyses using purified Pex7p and Pex21p variants will be needed in order to identify the rigidity threshold of the hydrophobic core necessary for PTS2-cargo transport.

Our crystal structure indicates that the N-terminal 44 residues of Pex7p allow protrusion of the bulge loop while simultaneously folding into a WD40-like structure to complete the rigid β-propeller structure. This adaptation differentiates Pex7p from other WD40 proteins. The

bulge loop is essential not only to form a landmark for Pex21p but also to constitute a part of the binding site for PTS2. Among the single–amino acid substitutions in human Pex7p that cause RCDP1[23,24] (Supplementary Fig. 1a), substitutions of His39 (Asn31 in *S. cerevisiae*) to Pro, and Gly41 (Gly33 in *S. cerevisiae*) to Val, are mutations on the bulge loop. This fact, together with the results of our mutation analyses of Pex7p Phe32 and Leu34, imply that the conserved shape and the surface property of the bulge loop are required for Pex7p's function.

The crystal structure suggests that Pex21p strengthens the binding of Pex7p to Fox3pN by directly attaching its C-terminal region onto the PTS2 binding site, rather than by some allosteric mechanism. We consider that this direct binding mechanism is not *S. cerevisiae*–specific but rather common to the co-receptor peroxins of other species, because the regions of Pex21p essential for formation of the recognition complex (Pex21p α1, α2, and α3) are conserved among other co-receptor peroxins (Supplementary Fig. 1b). Pex21p α1 is reminiscent of the finger loop of SRP54[40], in that Pex21p α1 forms a hydrophobic lid to cover the hydrophobic surface of PTS2 and stabilize the recognition complex. The importance of Pex21 α1 can be derived from the result that Pex21p ΔC and ΔL mutants could restore growth of *Δpex18Δpex21* on SCOT plates whereas Pex21p Δα1 mutant couldn't. The Pex7p–Fox3pN-bound structure of Pex21pC is likely to be induced on the complex formation.

If Pex21pC is separated from Pex7p and Fox3pN in aqueous solution, the exposure of the

hydrophobic residues and the lack of intra-molecular interactions will be unfavorable to

maintenance of the elongated structure of Pex21pC.

The crystal structure provides details regarding the complementarity between PTS2 and

the receptor complex. Because PTS2 folds into an α-helix, its hydrophobic key residues (Fox3p

Leu5, Ile8, Leu12) fit into the hydrophobic groove formed by both Pex7p and Pex21p, and its

hydrophilic key residues (Fox3p Arg4 and His11) fit into the hydrophilic groove on the top

surface of Pex7p. Whereas the hydrophobic key residues of PTS2 are recognized mainly by

spatial complementarity as parts of the hydrophobic core, the hydrophilic key residues of PTS2

are recognized both by spatial complementarity and by formation of salt bridges and hydrogen

bonds with Pex7p. Other helical N-terminal targeting signals, such as the signal peptide[40] and

mitochondrial targeting signal (MTS)[41], also contain hydrophobic residues in their sequence

motifs. However, the receptor proteins of the signal peptide and MTS (SRP54 and Tom20,

respectively) do not recognize any hydrophilic residue as specifically as Pex7p–Pex21p does.

The PTS2 system shares this characteristic with the PTS1 system, in which basic key residue of

the PTS1 sequence motif ($-[S/A/C]-[K/H/R]-[L/M]-CO_2^-$) is specifically recognized by

Pex5p[5,6]. It is reported that a mutated PTS1 peptide (Leu-Gln-Ser-Glu-Leu) has an affinity for

Pex5p two orders of magnitude lower than that of the wild-type PTS1 peptide

(Tyr-Gln-Ser-<u>Lys</u>-Leu)[6]. Consequently, both hydrophobic and hydrophilic key residues in

PTS1 and PTS2 achieve their specific complementarity with the receptors.

Our crystal structure supports several ideas presented in a recent modeling and mutational

study of the human Pex7p–PTS2 complex[25]. That study proposed that PTS2 forms an

amphipathic α-helix and binds to the top surface of Pex7p, and that the hydrophilic key residues

of PTS2 (Arg4 and His11 in *S. cerevisiae* Fox3p) interact with two glutamates in Pex7p

(Glu106 and Glu222 in *S. cerevisiae* Pex7p). However, because their model did not contain a

co-receptor peroxin, the bound surface of the modeled PTS2 helix is tilted compared with the

crystal structure. In the crystal structure, Fox3p Arg4 interacts with Pex7p Asp61 in addition to

Glu106, and Fox3p His11 mainly interacts with Pex7p Tyr178 and Tyr304 in addition to

Glu222. This explains the previous finding that Arg substitution of Glu222 (Glu200 in human

Pex7p) did not destroy the interaction completely, and that the corresponding mutant still

partially complemented Pex7p deficiency[25].

The first reported structure of the PTS2-recognition complex, presented here, provides a

structural framework for studying the import of PTS2-cargo into peroxisomes. Together with

previous reports of the PTS1 system, these findings deepen our understanding of peroxisomal

protein transport and reveal differences between peroxisomal targeting signals and those that

target proteins to other organelles. However, additional structures of PTS2-recognition

complexes containing other PTS2 sequences or containing Pex7p and the co-receptor peroxin

from other species will be required for a full understanding of the interactions among PTS2,

Pex7p, and the co-receptor peroxin.

Accession codes. Protein Data Bank: Coordinates and structure factors have been deposited with accession code 3W15.

AUTHOR CONTRIBUTIONS

D.P. generated plasmids, proteins, and crystals. D.P. and T.N. collected diffraction data and solved the structure. D.P. performed pull-down experiments and *in vivo* functional assays. H.K. supervised the project. D.P. and H.K. wrote the paper.

References for main text

1.   Wanders, R.J. & Waterham, H.R. Biochemistry of mammalian peroxisomes revisited. *Annu. Rev. Biochem.* **75**, 295-332 (2006).

2.   Platta, H.W. & Erdmann, R. Peroxisomal dynamics. *Trends Cell Biol.* **17**, 474-484 (2007).

3.   Ma, C., Agrawal, G. & Subramani, S. Peroxisome assembly: matrix and membrane protein biogenesis. *J. Cell Biol.* **193**, 7-16 (2011).

4.   Steinberg, S.J. et al. Peroxisome biogenesis disorders. *Biochim. Biophys. Acta* **1763**, 1733-1748 (2006).

5.   Stanley, W.A. et al. Recognition of a functional peroxisome type 1 target by the dynamic import receptor pex5p. *Mol. Cell* **24**, 653-663 (2006).

6.   Gatto, G.J., Jr., Geisbrecht, B.V., Gould, S.J. & Berg, J.M. Peroxisomal targeting signal-1 recognition by the TPR domains of human PEX5. *Nat. Struct. Biol.* **7**, 1091-1095 (2000).

7.   Lazarow, P.B. The import receptor Pex7p and the PTS2 targeting sequence. *Biochim. Biophys. Acta* **1763**, 1599-1604 (2006).

8.   Schliebs, W. & Kunau, W.H. PTS2 co-receptors: diverse proteins with common features. *Biochim. Biophys. Acta* **1763**, 1605-1612 (2006).

9.   Swinkels, B.W., Gould, S.J., Bodnar, A.G., Rachubinski, R.A. & Subramani, S. A novel, cleavable peroxisomal targeting signal at the amino-terminus of the rat 3-ketoacyl-CoA thiolase. *EMBO J.* **10**, 3255-3262 (1991).

10.   Osumi, T. et al. Amino-terminal presequence of the precursor of peroxisomal 3-ketoacyl-CoA thiolase is a cleavable signal peptide for peroxisomal targeting. *Biochem. Biophys. Res. Commun.* **181**, 947-954 (1991).

11.   Petriv, O.I., Tang, L., Titorenko, V.I. & Rachubinski, R.A. A new definition for the consensus sequence of the peroxisome targeting signal type 2. *J. Mol. Biol.* **341**, 119-134 (2004).

12.   Marzioch, M., Erdmann, R., Veenhuis, M. & Kunau, W.H. PAS7 encodes a novel yeast member of the WD-40 protein family essential for import of 3-oxoacyl-CoA thiolase, a PTS2-containing protein, into peroxisomes. *EMBO J.* **13**, 4908-4918 (1994).

13.   Zhang, J.W. & Lazarow, P.B. PEB1 (PAS7) in Saccharomyces cerevisiae encodes a hydrophilic, intra-peroxisomal protein that is a member of the WD repeat family and is essential for the import of thiolase into peroxisomes. *J. Cell Biol.* **129**, 65-80 (1995).

14. Braverman, N. et al. Human PEX7 encodes the peroxisomal PTS2 receptor and is responsible for rhizomelic chondrodysplasia punctata. *Nat. Genet.* **15**, 369-376 (1997).

15. Motley, A.M. et al. Rhizomelic chondrodysplasia punctata is a peroxisomal protein targeting disease caused by a non-functional PTS2 receptor. *Nat. Genet.* **15**, 377-380 (1997).

16. Purdue, P.E., Zhang, J.W., Skoneczny, M. & Lazarow, P.B. Rhizomelic chondrodysplasia punctata is caused by deficiency of human PEX7, a homologue of the yeast PTS2 receptor. *Nat. Genet.* **15**, 381-384 (1997).

17. Elgersma, Y. et al. A mobile PTS2 receptor for peroxisomal protein import in Pichia pastoris. *J. Cell Biol.* **140**, 807-820 (1998).

18. Mukai, S., Ghaedi, K. & Fujiki, Y. Intracellular localization, function, and dysfunction of the peroxisome-targeting signal type 2 receptor, Pex7p, in mammalian cells. *J. Biol. Chem.* **277**, 9548-9561 (2002).

19. Nito, K., Hayashi, M. & Nishimura, M. Direct interaction and determination of binding domains among peroxisomal import factors in Arabidopsis thaliana. *Plant Cell Physiol.* **43**, 355-366 (2002).

20. Sichting, M., Schell-Steven, A., Prokisch, H., Erdmann, R. & Rottensteiner, H. Pex7p and Pex20p of Neurospora crassa function together in PTS2-dependent protein import into peroxisomes. *Mol. Biol. Cell* **14**, 810-821 (2003).

21. Rehling, P. et al. The import receptor for the peroxisomal targeting signal 2 (PTS2) in Saccharomyces cerevisiae is encoded by the PAS7 gene. *EMBO J.* **15**, 2901-2913 (1996).

22. Glover, J.R., Andrews, D.W., Subramani, S. & Rachubinski, R.A. Mutagenesis of the amino targeting signal of Saccharomyces cerevisiae 3-ketoacyl-CoA thiolase reveals conserved amino acids required for import into peroxisomes in vivo. *J. Biol. Chem.* **269**, 7558--7563 (1994).

23. Braverman, N. et al. Mutation analysis of PEX7 in 60 probands with rhizomelic chondrodysplasia punctata and functional correlations of genotype with phenotype. *Hum. Mutat.* **20**, 284-297 (2002).

24. Motley, A.M. et al. Mutational spectrum in the PEX7 gene and functional analysis of mutant alleles in 78 patients with rhizomelic chondrodysplasia punctata type 1. *Am. J. Hum. Genet.* **70**, 612-624 (2002).

25. Kunze, M. et al. Structural requirements for interaction of peroxisomal targeting signal 2 and its receptor PEX7. *J. Biol. Chem.* **286**, 45048-45062 (2011).

26. Purdue, P.E., Yang, X. & Lazarow, P.B. Pex18p and Pex21p, a novel pair of related

peroxins essential for peroxisomal targeting by the PTS2 pathway. *J. Cell Biol.* **143**, 1859-1869 (1998).

27. Einwachter, H., Sowinski, S., Kunau, W.H. & Schliebs, W. Yarrowia lipolytica Pex20p, Saccharomyces cerevisiae Pex18p/Pex21p and mammalian Pex5pL fulfil a common function in the early steps of the peroxisomal PTS2 import pathway. *EMBO Rep.* **2**, 1035-1039 (2001).

28. Leon, S. et al. Dynamics of the peroxisomal import cycle of PpPex20p: ubiquitin-dependent localization and regulation. *J. Cell Biol.* **172**, 67-78 (2006).

29. Khan, B.R. & Zolman, B.K. pex5 Mutants that differentially disrupt PTS1 and PTS2 peroxisomal matrix protein import in Arabidopsis. *Plant Physiol.* **154**, 1602-1615 (2010).

30. Braverman, N., Dodt, G., Gould, S.J. & Valle, D. An isoform of pex5p, the human PTS1 receptor, is required for the import of PTS2 proteins into peroxisomes. *Hum. Mol. Genet.* **7**, 1195-1205 (1998).

31. Otera, H. et al. Peroxisome targeting signal type 1 (PTS1) receptor is involved in import of both PTS1 and PTS2: studies with PEX5-defective CHO cell mutants. *Mol. Cell Biol.* **18**, 388-399 (1998).

32. Matsumura, T., Otera, H. & Fujiki, Y. Disruption of the interaction of the longer isoform of Pex5p, Pex5pL, with Pex7p abolishes peroxisome targeting signal type 2 protein import in mammals. Study with a novel Pex5-impaired Chinese hamster ovary cell mutant. *J. Biol. Chem.* **275**, 21715-21721 (2000).

33. Dodt, G., Warren, D., Becker, E., Rehling, P. & Gould, S.J. Domain mapping of human PEX5 reveals functional and structural similarities to Saccharomyces cerevisiae Pex18p and Pex21p. *J. Biol. Chem.* **276**, 41769-41781 (2001).

34. Leon, S. & Subramani, S. A conserved cysteine residue of Pichia pastoris Pex20p is essential for its recycling from the peroxisome to the cytosol. *J. Biol. Chem.* **282**, 7424-7430 (2007).

35. Hensel, A. et al. Cysteine-dependent ubiquitination of Pex18p is linked to cargo translocation across the peroxisomal membrane. *J. Biol. Chem.* **286**, 43495-43505 (2011).

36. Neufeld, C. et al. Structural basis for competitive interactions of Pex14 with the import receptors Pex5 and Pex19. *EMBO J.* **28**, 745-754 (2009).

37. Smith, T.F., Gaitatzes, C., Saxena, K. & Neer, E.J. The WD repeat: a common architecture for diverse functions. *Trends Biochem. Sci.* **24**, 181-185 (1999).

38. Wall, M.A. et al. The structure of the G protein heterotrimer Gi alpha 1 beta 1 gamma 2.

Cell **83**, 1047-1058 (1995).

39. Couture, J.F., Collazo, E. & Trievel, R.C. Molecular recognition of histone H3 by the WD40 protein WDR5. *Nat. Struct. Mol. Biol.* **13**, 698-703 (2006).

40. Janda, C.Y. et al. Recognition of a signal peptide by the signal recognition particle. *Nature* **465**, 507-510 (2010).

41. Abe, Y. et al. Structural basis of presequence recognition by the mitochondrial protein import receptor Tom20. *Cell* **100**, 551-560 (2000).

42. Baker, N.A., Sept, D., Joseph, S., Holst, M.J. & McCammon, J.A. Electrostatics of nanosystems: application to microtubules and the ribosome. *Proc. Natl. Acad. Sci. USA* **98**, 10037-10041 (2001).

Figure legends

Figure 1

Structure of the Pex7p–Pex21pC–Fox3pN-MBP complex. (a) Schematic diagrams of the constructs used for crystallization. The color code here is used for all figures, unless otherwise noted. WD1–6 indicate WD40 motifs. ND, N-terminal conserved domain; WF, Wxxx[F/Y] Pex14p-binding motif; Pex7pBD, Pex7p-binding domain. (b) Skeleton representation of the hetero-trimer in the crystallographic asymmetric unit. (c) Ribbon and surface representations of the side view (left) and the top view (right) of the hetero-trimer Pex7p–Pex21pC–Fox3pN. Side chains of Arg4, Leu5, His11, and Leu12 are shown as stick models. The disordered loops (DLs) in Pex7p and Pex21pC are presented as dashed curves. The red arrow in the leftmost panel represents the viewpoint of the left panel in Fig. 3b and the viewpoint of Fig. 4c. Nt, N-terminus; Ct, C-terminus.

Figure 2

Cooperative complex formation of Fox3p, Pex7p, and Pex21pC. The results of pull-down experiments using glutathione sepharose resin (a) or amylose resin (b) to examine all combinations of complex formation between any two or all three of Fox3p, Pex7p, and

Pex21pC are shown. Proteins were mixed at 5 μM with 15 μl of resin in buffer. The input and

bound fractions were analyzed by SDS-PAGE and stained with Coomassie Brilliant Blue.

Figure 3

Pex7p–Pex21pC receptor complex formation. (a) Open-book representation of Pex7p and

Pex21pC. Pex7p is in the same orientation as in the right panel of Fig. 1c. Pex21pC is in the

orientation rotated by 135° from the orientation in the right panel of Fig. 1c. Fox3pN is shown

as a ribbon model in yellow, and the side-chains of Met1, Arg4, Leu5, Ile8, His11, and Leu12

are shown to indicate its orientation. Electrostatic surfaces of Pex7p and Pex21pC were colored

according to local surface properties using PyMOL with the APBS[42] plugin. Surface regions of

positive potential are colored blue, regions of negative potential red, and neutral regions white.

The color ramp is from $-3kT$ to $+3kT$, where k is the Boltzmann constant and T is the absolute

temperature. The dashed boxes indicate the hydrophobic interfaces important for

Pex7p–Pex21p complex formation. In particular, the dashed box on Pex7p indicates the

hydrophobic ridge. The dashed circle indicates the bulge loop. (b) Residues forming

hydrophobic interfaces between Pex7p and Pex21pC are shown in the left panel, and residues

forming electrostatic interactions between Pex7p and Pex21pC in the right panel. The

viewpoint of the left panel is indicated in Fig. 1c by a red arrow, and the helix of Fox3pN is

omitted from the left panel for clarity. Dashed black lines indicate possible hydrogen bonds.

Figure 4

Molecular recognition of key residues of PTS2. (a) The amphipathic α-helix of Fox3pN.

Hydrophobic residues are highlighted by underlines. (b) Stereo view of the PTS2 binding

pocket. The side chains of Met1, Arg4, Leu5, Ile8, His11, and Leu12 of Fox3pN are shown.

Dashed black lines indicate possible hydrogen bonds. (c) The surface of the PTS2-binding

pocket is shown and colored according to the peptide chain (Pex21pC, light pink; Pex7p, pale

green) in the left panel, and colored according to local electrostatic properties as in Fig. 3a in

the right panel. The viewpoint is indicated in Fig. 1c by a red arrow. The dashed box indicates

the hydrophobic groove, and the dashed ellipse indicates the hydrophilic groove.

Figure 5

Functional assays of Pex7p and Pex21p variants. (a, b) The results of pull-down experiments

with amylose resin to examine the ability of variants of Pex21pC (a) and Pex7p (b) to form the

ternary complex. (c) Growth assays of the *S. cerevisiae* strains on SCOT agar plates (oleic acid

is the only carbon source) or SCDT agar plates (glucose is the only carbon source). Ten-fold

serial dilutions of the strains were spotted onto the agar plates and incubated at 30°C for one

week (SCOT) or one day (SCDT). Approximate numbers of cells per spot are indicated. WT,

wild type.

Table 1. Data collection and refinement statistics

	Pex7p(Δ257–265)–Pex21pC–Fox3pN-MBP
Data collection	
Space group	$P2_1$
Cell dimensions	
a, b, c (Å)	78.9, 52.8, 97.6
α, β, γ (°)	90, 106.6, 90
Resolution (Å)	32.2–1.8 (1.90–1.80)*
R_{merge}	0.066 (0.199)
$I / \sigma I$	20.2 (8.8)
Completeness (%)	99.8 (99.2)
Redundancy	7.1 (6.9)
Refinement	
Resolution (Å)	32.2–1.80
No. reflections	67,828
R_{work} / R_{free}	0.189/0.224
No. atoms	
Protein	6,219
Ligand/ion	42
Water	563
B-factors	
Protein	20.87
Ligand/ion	34.13
Water	26.45
r.m.s. deviations	
Bond lengths (Å)	0.008
Bond angles (°)	1.063

*Values in parentheses are for the highest-resolution shell.

Online Methods

Plasmids. The details of plasmids used in this study are described in Supplementary Note and

Supplementary Table 1.

Expression and purification of Pex7p and its variants. *P. pastoris* plasmids for expression of

N-terminally GST-tagged Pex7p and its variants were linearized with PmeI (NEB) and

transformed into *P. pastoris* strain SMD1163 (Invitrogen) as described[43]. Positive

transformants were selected using YPD (1% yeast extract, 2% peptone, 2% dextrose) agar

plates containing 300 μg ml^{-1} Zeocin. The colonies were grown at 30°C to an OD_{600} of 5 in

YPD medium, and 20 ml of this culture was used to inoculate 1 l of methanol induction medium

(1% methanol, 1% yeast extract, 1.5% peptone, 1.34% yeast nitrogen base with ammonium

sulfate without amino acids, 0.5% sorbitol, 4×10^{-5}% biotin) in 5-l baffled flasks. The cells were

grown at 30°C with vigorous shaking. Methanol was added to a concentration of 0.7% after 16

h of induction, and cells were harvested after additional culture for 4 h.

Protein samples were kept at 4°C during all subsequent steps. Harvested cells (90 g) were

suspended in 250 ml buffer A (30 mM Tris-HCl pH 7.5, 500 mM NaCl, 5% glycerol, 0.05%

Tween 20, 1 mM DTT, 1 mM PMSF) and lysed with an Emulsiflex-C3 high-pressure

homogenizer (Avestin). Clarified lysate was incubated with 3 ml Glutathione Sepharose 4B

resin (GE Healthcare) overnight. After washing the resin with 50 column volumes (CVs) of

buffer B (30 mM Tris-HCl pH 7.5, 300 mM NaCl, 1 mM DTT), His_6-tagged TEV protease was

mixed with the resin and 1 CV of buffer B overnight to remove the GST-tag and release Pex7p

from the resin. The supernatant was passed through 1 ml Ni-IMAC (Bio-Rad) column to

remove TEV protease, and the unbound fraction containing Pex7p was applied to a HiLoad

16/60 Superdex 200 pg gel filtration column (GE Healthcare) equilibrated with buffer B. Peak

fractions containing Pex7p were pooled, concentrated with Amicon Ultra Centrifugal Filters

(Millipore), flash-frozen in liquid nitrogen, and stored at $-80°C$. The yield of Pex7p was 0.4 mg

per liter of culture.

Expression and purification of Pex21pC, Fox3p, Fox3pN-MBP, and MBP-Pex21pC. *E.*

coli BL21(DE3) cells transformed with plasmids for expression of N-terminally GST-tagged

Pex21pC, Fox3p, or Fox3pN-MBP were grown in LB medium at 37°C to an OD_{600} of 0.6.

Protein expression was induced with 0.5 mM IPTG for 4 h at 37°C. Harvested cells (10 g) were

suspended in 80 ml buffer C (30 mM Tris-HCl pH 7.5, 150 mM NaCl, 1 mM DTT) containing

1 mM PMSF and lysed by sonication on ice. Further purification after disruption of the cells

was performed using the same procedure as for purification of Pex7p described above, except that buffer C was used for washing the resin and gel filtration chromatography. Purified Pex21pC, Fox3p, and Fox3pN-MBP were concentrated in buffer C, flash-frozen, and stored at −80°C. The yield of Pex21pC, Fox3p, and Fox3pN-MBP were 2, 10, and >20 mg per liter of culture, respectively.

E. coli BL21(DE3) cells transformed with plasmids for expression of C-terminally His$_6$-tagged MBP-Pex21pC and its variants were cultured in the same way as cells expressing GST-tagged Pex21pC. Harvested cells (1 g) were suspended in 25 ml buffer B and lysed by sonication on ice. Clarified lysate was supplied with imidazole to a concentration of 20 mM and applied on 1 ml Ni-IMAC column. The resin was washed with 25 CVs of buffer B containing 20 mM imidazole and MBP-Pex21pC was eluted with buffer B containing 400 mM imidazole. Eluted proteins were concentrated in buffer B, flash frozen and stored at −80°C.

Crystallization of Pex7p(Δ257–265)–Pex21pC–Fox3pN-MBP hetero-trimer. Purified Pex7p(Δ257–265) (2 mg), Pex21pC (1 mg), and Fox3pN-MBP (4 mg) were mixed in 4 ml buffer B, incubated overnight at 4°C, and subjected to gel filtration chromatography on a HiLoad 16/60 Superdex 200 pg column with buffer C. The peak fractions containing the ternary

complex were confirmed by SDS-PAGE, and concentrated in buffer C to 14 mg ml^{-1}. Crystals

were grown at 20°C by hanging-drop vapor diffusion, mixing 1 μl of the protein solution and 1

μl of the reservoir solution containing 25% PEG2000, 0.3 M magnesium nitrate, and 0.1 M

Tris-HCl (pH 7.7). Plate crystals appeared in a week and reached their maximal size (0.5 × 0.2

× 0.02 mm) within one month.

Data collection and structure determination. The crystals were serially transferred to

cryoprotectant solutions (25–35% PEG2000, 0.1 M NaCl, 0.3 M magnesium nitrate, 0.1 M

Tris-HCl pH 7.5) and soaked in the final solution for 1 h before flash-freezing in liquid nitrogen.

A 1.8-Å resolution dataset was collected from a single crystal at 100 K at the SPring-8 beamline

BL41XU at a wavelength of 1.0000 Å and processed using the iMOSFLM[44] and CCP4

software[45]. Initial phases were solved by molecular replacement with PHASER[46], using crystal

structures of MBP (PDB entry 1OMP) and human WDR5 (PDB entry 2H13) as search models.

ARP/wARP[47] was used to build the initial model. Incomplete parts of the model were manually

built using Coot[48] and refined using REFMAC5[49] to R/R_{free} values of 0.189/0.224 at 1.8 Å

resolution. As validated with MolProbity[50], 97.8% of the residues were in the favored region of

the Ramachandran plot, and the rest were in the allowed region. Data collection and refinement

statistics are summarized in Table 1. All structural figures were generated using PyMOL

(http://www.pymol.org). PISA[51] was used to analyze intermolecular interactions and to

calculate the surface areas.

GST- and MBP-pull-down experiments. Proteins were diluted to 5 µM each in 100 µl of

buffer B containing 0.01% Tween 20. Four-fifths of the mixture was incubated with 15 µl of

Glutathione Sepharose 4B resin or amylose resin (NEB) at 4°C for 1 h, and the remaining 20 µl

was kept as the input fraction and mixed with 5 µl of 5× sample buffer. The resin was washed

three times with 500 µl buffer B containing 0.01% Tween 20, and the bound fraction was eluted

by mixing the resin with 30 µl 2× sample buffer. The input fraction and the bound fractions

were analyzed by SDS-PAGE and stained with Coomassie Brilliant Blue.

***S. cerevisiae* strains and complementation assays.** All *S. cerevisiae* strains used in this study

were generated from strain BY20134 (W303-1A background), which was provided by the

National Bio-Resource Project (NBRP) of the MEXT, Japan. Gene deletion was performed

using the one-step PCR method as described[52]. *PEX7* was replaced with the *URA3* gene to

generate strain *Δpex7*. *PEX21* and *PEX18* were replaced serially with the *LEU2* and *HIS3* genes,

respectively, to generate strain *Δpex18Δpex21*. All deletions were confirmed by colony PCR on

genomic DNA. Plasmids were transformed into BY20134, *Δpex7*, and *Δpex18Δpex21* strains as

described[53], and transformants were selected on SCD (0.67% yeast nitrogen base with

ammonium sulfate without amino acids, 2% dextrose supplemented with amino acids, adenine,

and uracil) agar plates lacking the appropriate amino acids and/or uracil. BY20134 strain

transformed with pAG304-Fox3pN-EGFP/mCherry-PTS1 is referred as BY20134EM. The list

of all *S. cerevisiae* strains used in this study is presented on Supplementary Table 2.

Growth assays of *S. cerevisiae* strains were performed as described previously[26] with

minor modifications. The cells of each strain were grown at 30°C to an OD_{600} of 2 in SCEO

medium (0.67% yeast nitrogen base with ammonium sulfate without amino acids, 2% (v/v)

ethanol, 0.1% (w/v) oleic acid, 0.4% (w/v) Tween 40, appropriate amino acids, uracil, and

adenine). The cells were washed with distilled water and applied at ten-fold serial dilutions to

SCOT (0.67% yeast nitrogen base with ammonium sulfate without amino acids, 0.1% (w/v)

oleic acid, 0.4% (w/v) Tween 40, amino acids, uracil, and adenine) and SCDT (0.67% yeast

nitrogen base with ammonium sulfate without amino acids, 2% dextrose, 0.4% (w/v) Tween 40,

amino acids, uracil, and adenine) agar plates and incubated at 30°C. Aliquots of the cells were

also used for western blotting (Supplementary Fig. 5b and Supplementary Note) and

visualization on a confocal fluorescence microscope (A1, Nikon).

References for Online Methods

43. Wu, S. & Letchworth, G.J. High efficiency transformation by electroporation of Pichia pastoris pretreated with lithium acetate and dithiothreitol. *Biotechniques* **36**, 152-154 (2004).

44. Battye, T.G., Kontogiannis, L., Johnson, O., Powell, H.R. & Leslie, A.G. iMOSFLM: a new graphical interface for diffraction-image processing with MOSFLM. *Acta Crystallogr. D Biol. Crystallogr.* **67**, 271-281 (2011).

45. Winn, M.D. et al. Overview of the CCP4 suite and current developments. *Acta Crystallogr. D Biol. Crystallogr.* **67**, 235-242 (2011).

46. McCoy, A.J. et al. Phaser crystallographic software. *J. Appl. Crystallogr.* **40**, 658-674 (2007).

47. Perrakis, A., Morris, R. & Lamzin, V.S. Automated protein model building combined with iterative structure refinement. *Nat. Struct. Biol.* **6**, 458-463 (1999).

48. Emsley, P. & Cowtan, K. Coot: model-building tools for molecular graphics. *Acta Crystallogr. D Biol. Crystallogr.* **60**, 2126-2132 (2004).

49. Murshudov, G.N., Vagin, A.A. & Dodson, E.J. Refinement of macromolecular structures by the maximum-likelihood method. *Acta Crystallogr. D Biol. Crystallogr.* **53**, 240-255 (1997).

50. Chen, V.B. et al. MolProbity: all-atom structure validation for macromolecular crystallography. *Acta Crystallogr. D Biol. Crystallogr.* **66**, 12-21 (2010).

51. Krissinel, E. & Henrick, K. Inference of macromolecular assemblies from crystalline state. *J. Mol. Biol.* **372**, 774-797 (2007).

52. Baudin, A., Ozier-Kalogeropoulos, O., Denouel, A., Lacroute, F. & Cullin, C. A simple and efficient method for direct gene deletion in Saccharomyces cerevisiae. *Nucleic Acids Res.* **21**, 3329-3330 (1993).

53. Gietz, R.D. & Schiestl, R.H. Frozen competent yeast cells that can be transformed with high efficiency using the LiAc/SS carrier DNA/PEG method. *Nat. Protoc.* **2**, 1-4 (2007).
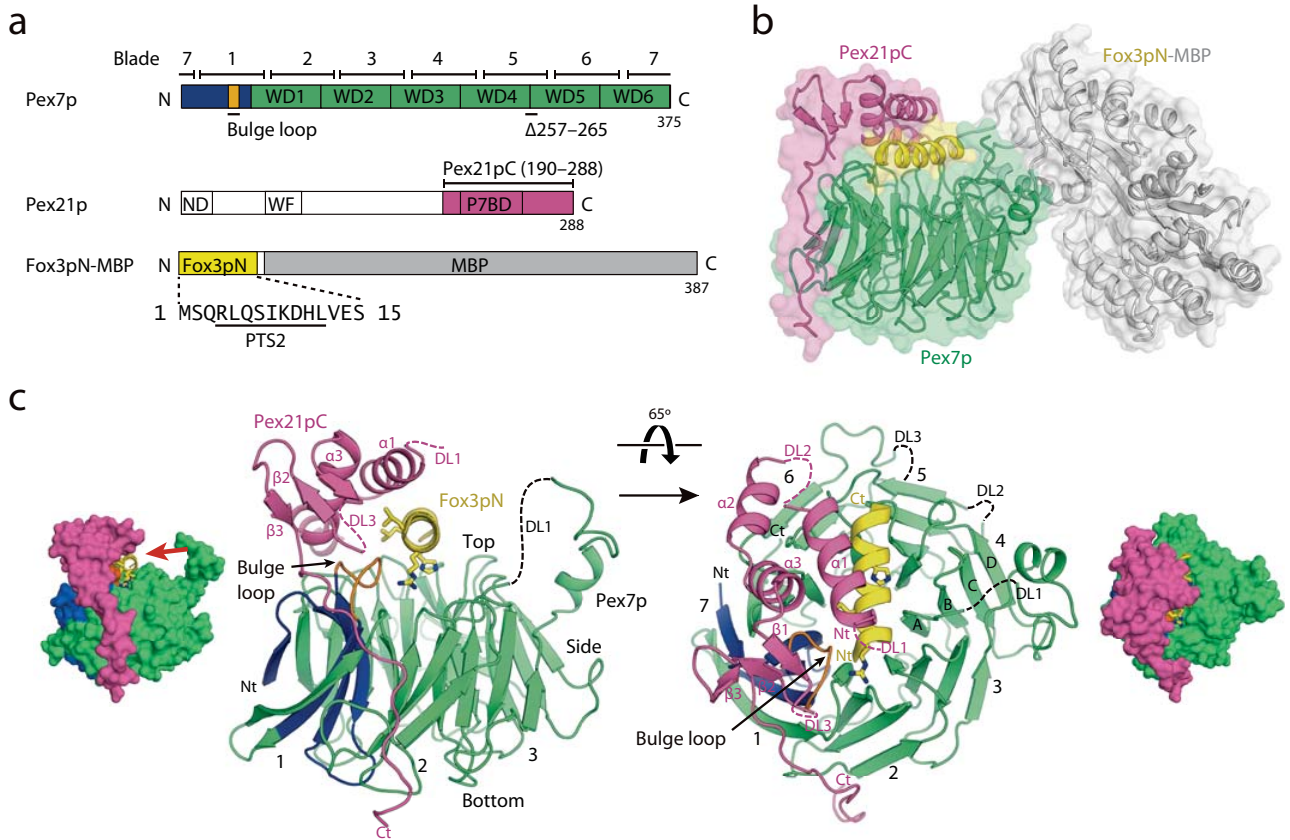
a

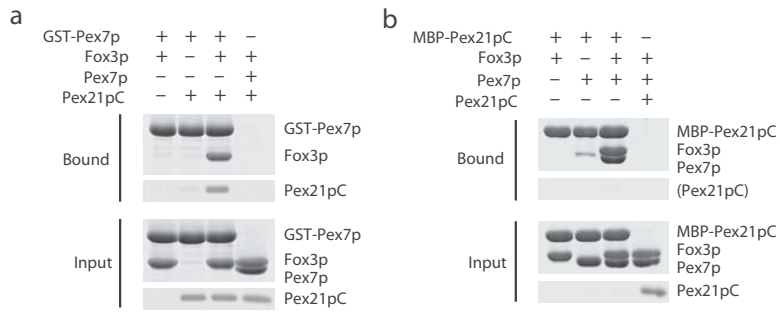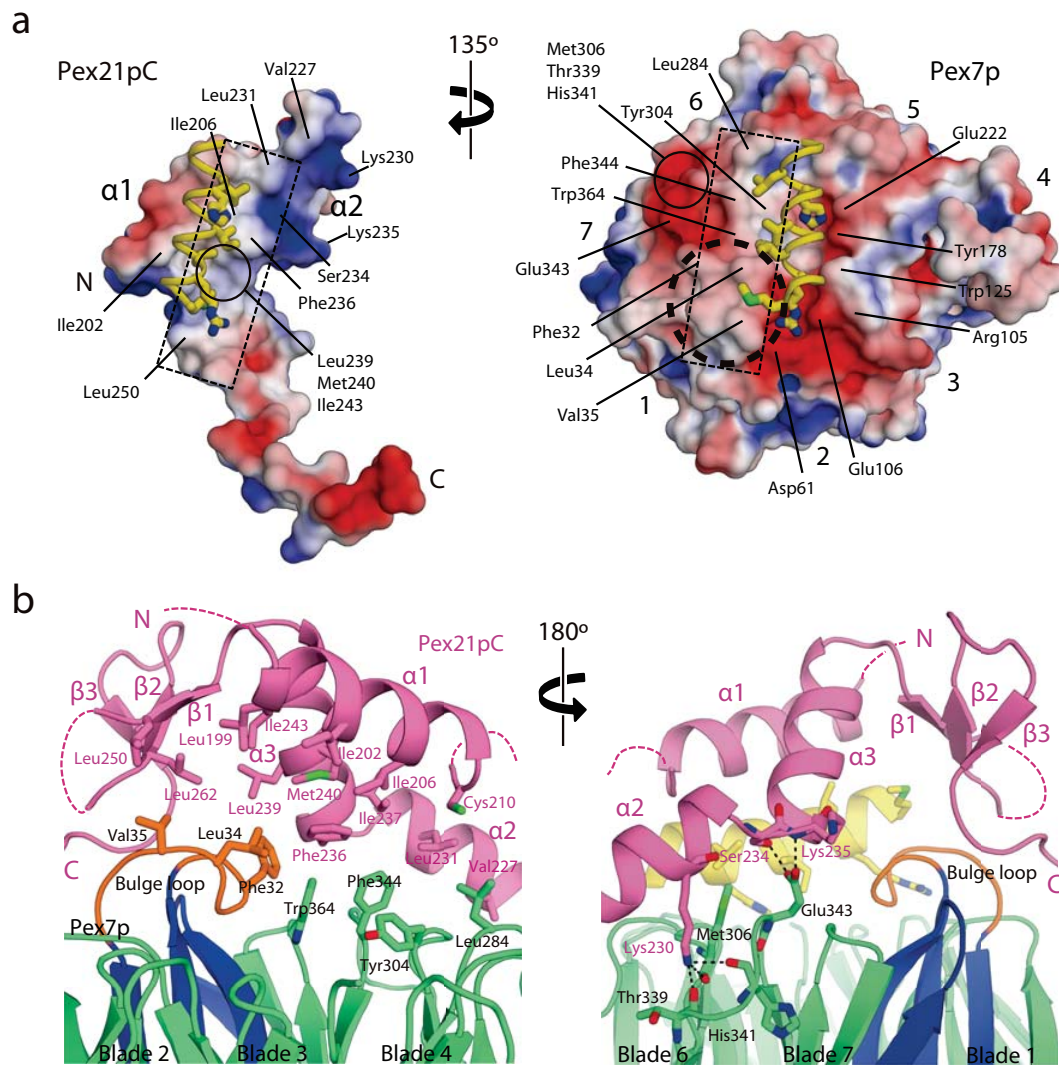Blade 7 1 2 3 4 5 6 7

Pex7p N [WD1 WD2 WD3 WD4 WD5 WD6] C

Bulge loop Δ257–265 375

Pex21p N [ND] [WF] [P7BD] C

Pex21pC (190–288)

288

Fox3pN-MBP N [Fox3pN] [MBP] C

387

1 MSQRLQSIKDHLVES 15

PTS2

b

Pex21pC   Fox3pN-MBP

Pex7p

c

Figure-1, Kato

a

GST-Pex7p	+	+	+	−
Fox3p	+	−	+	+
Pex7p	−	−	−	+
Pex21pC	−	+	+	+

Bound

GST-Pex7p
Fox3p

Pex21pC

Input

GST-Pex7p
Fox3p
Pex7p

Pex21pC

b

MBP-Pex21pC	+	+	+	−
Fox3p	+	−	+	+
Pex7p	−	+	+	+
Pex21pC	−	−	−	+

Bound

MBP-Pex21pC
Fox3p
Pex7p

(Pex21pC)

Input

MBP-Pex21pC
Fox3p
Pex7p

Pex21pC

Figure-2, Kato

a

Pex21pC

Val227
Leu231
Ile206
Lys230
α1
α2
Lys235
N
Ser234
Phe236
Ile202
Leu250
Leu239
Met240
Ile243
C

135°

Met306
Thr339
His341
Leu284
Tyr304
6
Pex7p
5
Phe344
Glu222
Trp364
7
4
Glu343
Tyr178
Phe32
Trp125
Leu34
Arg105
Val35
1
3
2
Glu106
Asp61

b

N
Pex21pC
β2
β3
α1
β1
Ile243
Leu199
α3
Ile202
Leu250
Met240
Ile206
Cys210
Leu262
Leu239
Ile237
α2
Val35
Phe236
Leu231
Val227
Val35
Leu34
Phe32
Bulge loop
Phe344
Pex7p
Trp364
Tyr304
Leu284
Blade 2
Blade 3
Blade 4

180°

N
α1
β1
β2
α3
β3
α2
Ser234
Lys235
Bulge loop
C
Glu343
Lys230
Met306
Thr339
His341
Blade 6
Blade 7
Blade 1

Figure-3, Kato

Figure-4, Kato
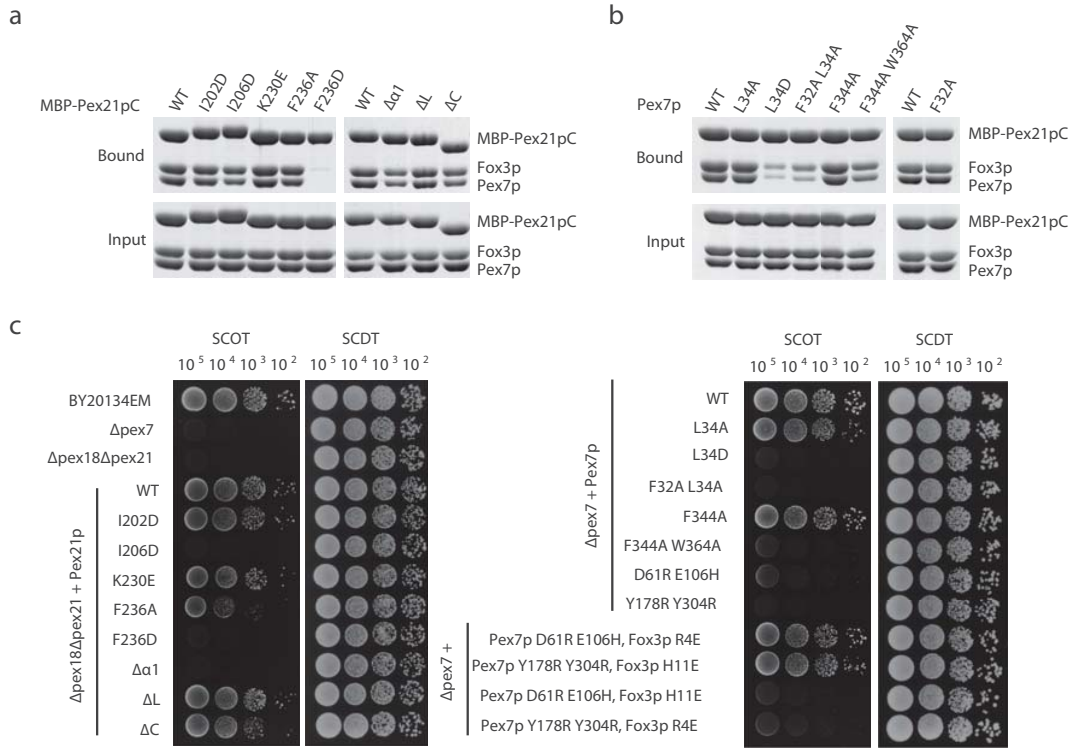
Figure-5, Kato
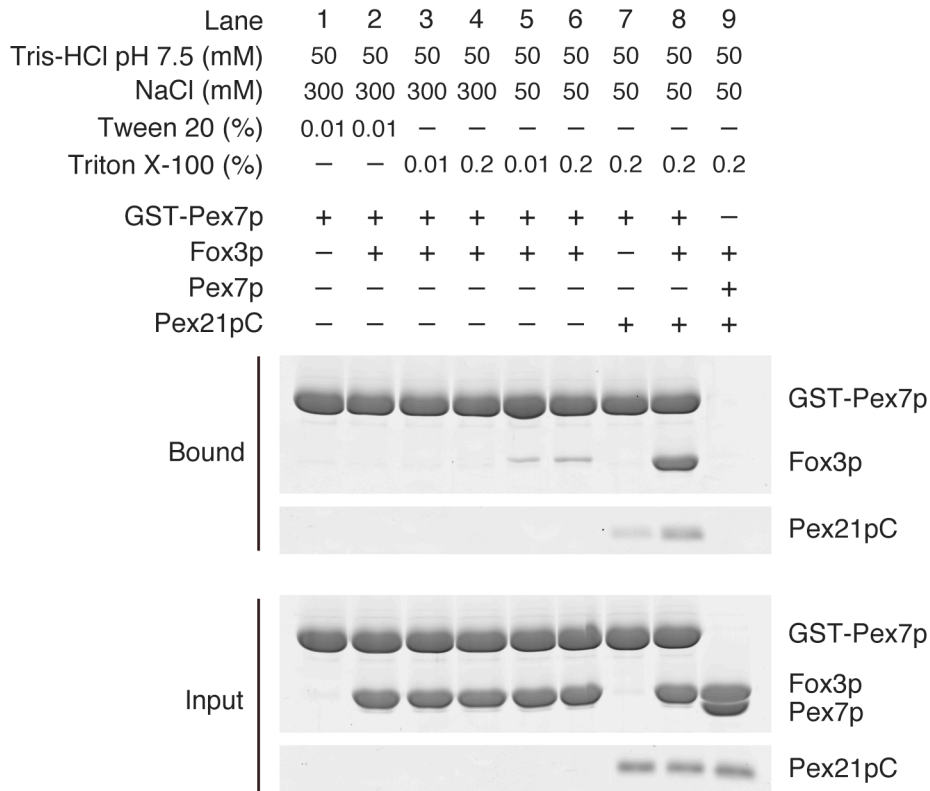
Supplementary Figure 1

Amino acid sequence alignments and conserved residues.
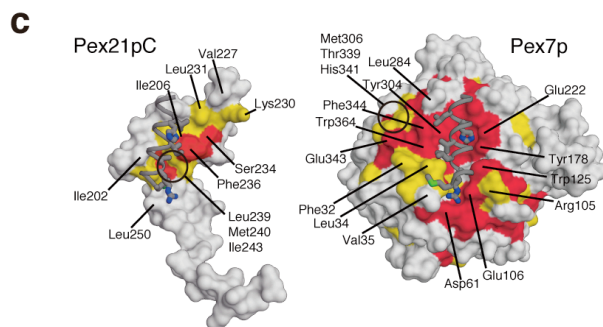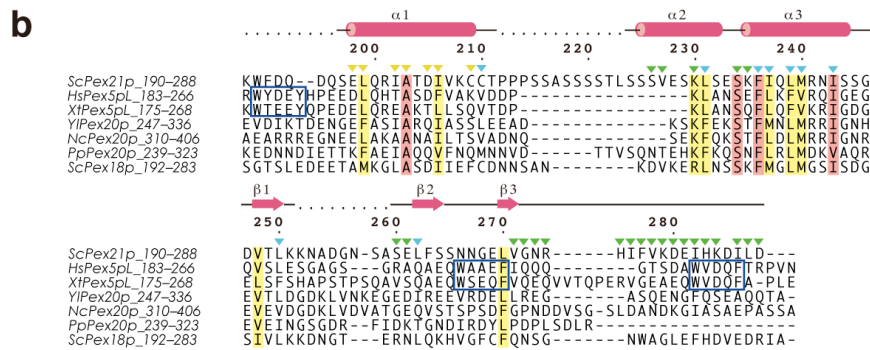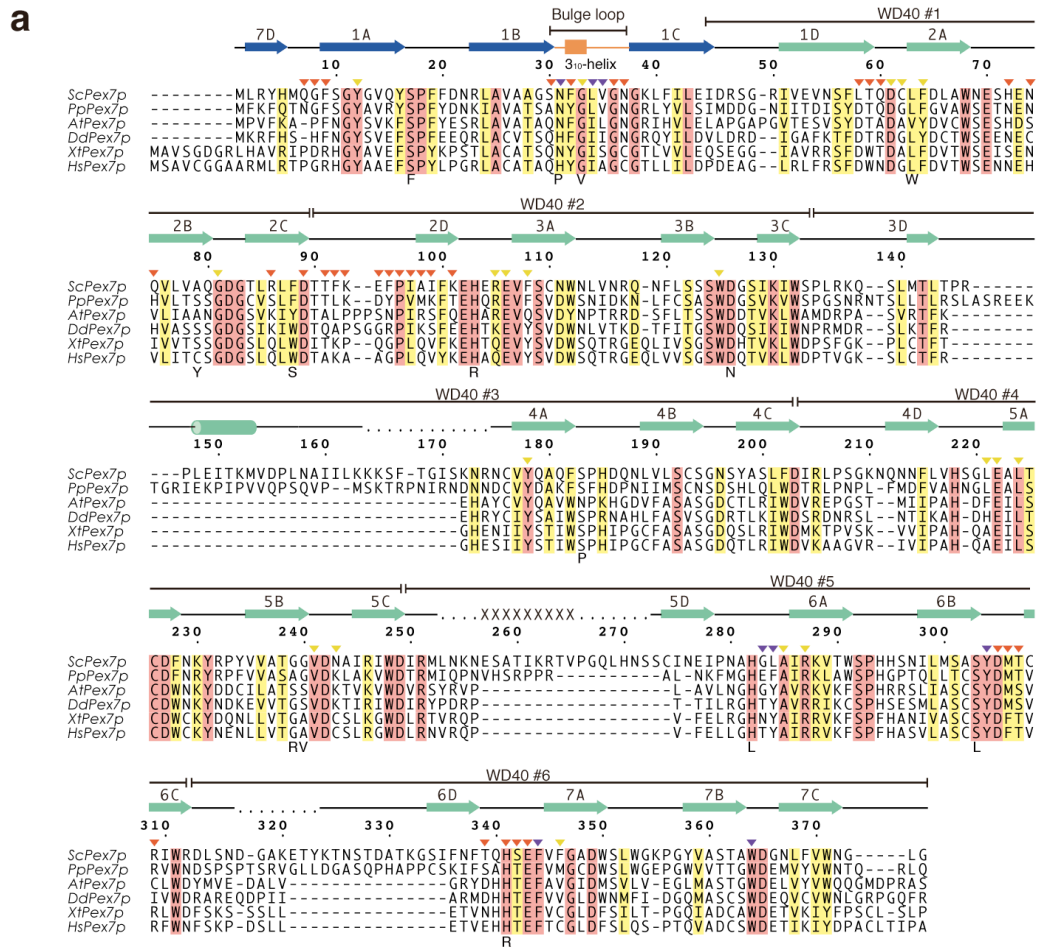
Sequence alignments of (a) six Pex7p homologs, and (b) the homologous regions of co-receptor peroxins for PTS2 and Pex7p binding. Sc, *Saccharomyces cerevisiae*; Pp, *Pichia pastoris*; At, *Arabidopsis thaliana*; Dd, *Dictyostelium discoideum*; Xt, *Xenopus tropicalis*; Hs, *Homo sapiens*; Yl, *Yarrowia lipolytica*; Nc, *Neurospora crassa*. Alignments were performed with ClustalW 1.83[1] and manually adjusted. Residues that are identical in all sequences are shaded red, and residues that only have conserved substitutions are shaded yellow. Secondary-structure elements and residue numbering of Pex7p and Pex21pC are indicated above the alignments. Point mutations of human Pex7p that cause RCDP1[2,3] are indicated below the sequence of HsPex7p. In (a, b), "." indicates a residue missing electron density; "X" indicates a residue deleted to optimize crystal quality. Down-pointing triangles indicate the interface residues, and are colored as follows: residues of Pex7p and Pex21p that only interact with Fox3pN are yellow; residues of Pex7p that interact with Pex21p are red; residues of Pex7p that interact with both Fox3pN and Pex21p are purple; residues of Pex21p that interact with Pex7p are green; and residues of Pex21p that interact with both Fox3pN and Pex7p are cyan. Blue-boxed regions in (b) indicate the Pex14p-binding motif. (c) Surface representation of Pex21pC and Pex7p. The surfaces of conserved residues are highlighted as in (a, b) according to their conservation.

Supplementary Figure 2

Fox3p binds to Pex7p with higher affinity in the lower salt environment.

Lane	1	2	3	4	5	6	7	8	9
Tris-HCl pH 7.5 (mM)	50	50	50	50	50	50	50	50	50
NaCl (mM)	300	300	300	300	50	50	50	50	50
Tween 20 (%)	0.01	0.01	−	−	−	−	−	−	−
Triton X-100 (%)	−	−	0.01	0.2	0.01	0.2	0.2	0.2	0.2
GST-Pex7p	+	+	+	+	+	+	+	+	−
Fox3p	−	+	+	+	+	+	−	+	+
Pex7p	−	−	−	−	−	−	−	−	+
Pex21pC	−	−	−	−	−	−	+	+	+

Pull-down experiments were performed using glutathione sepharose resin under the procedure described in the Online Methods section. Proteins were diluted to 5 μM in buffers containing 50 mM Tris-HCl pH 7.5 and different concentrations of NaCl, Tween 20, and Triton X-100 indicated in the figure. The input and bound fractions were analyzed by SDS-PAGE and stained with Coomassie Brilliant Blue. The buffer composition for the experiment of lane 6 was based on the solution A described previously[4].

Supplementary Figure 3

Electron-density maps around the PTS2-recognition site.
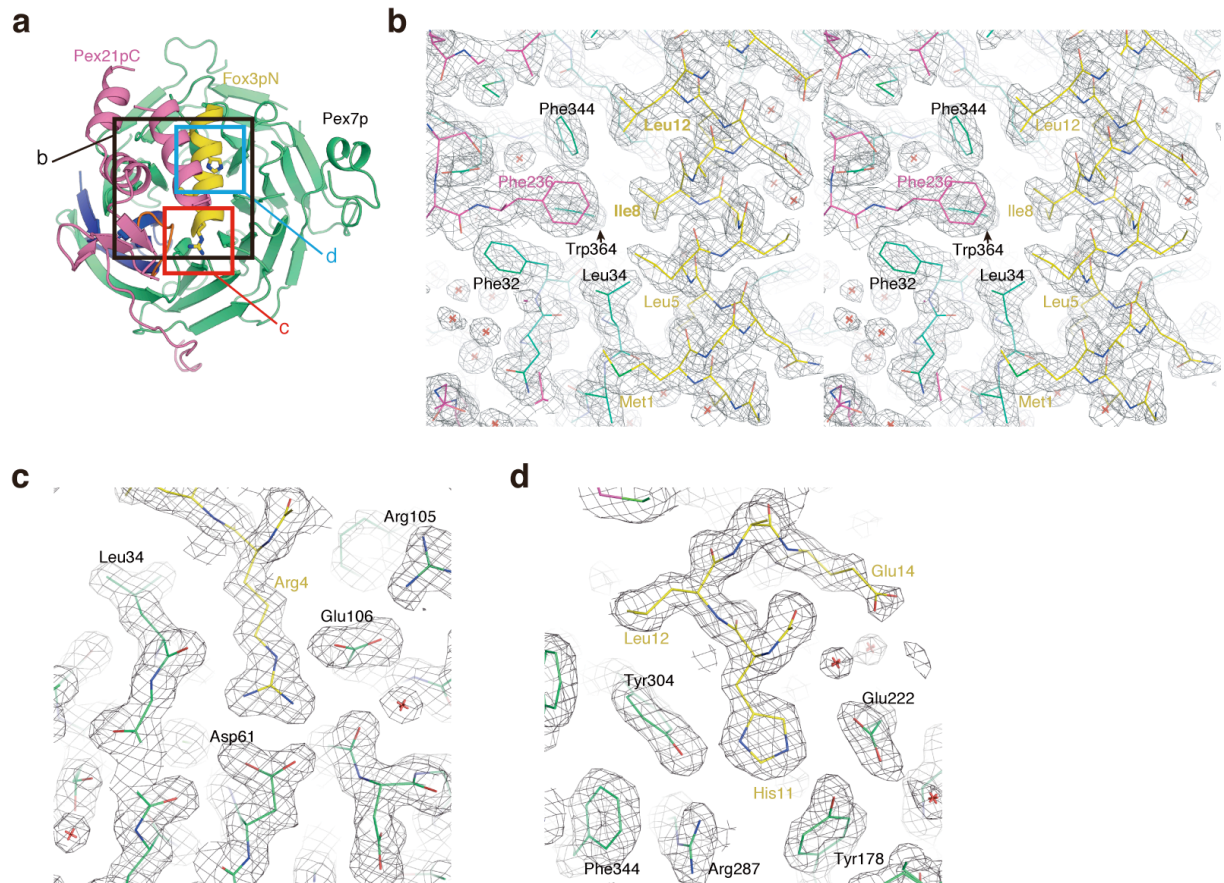
(a) The same ribbon presentation as in Fig. 1c, right. Boxes indicate the regions enlarged in (b, c, d). (b–d) Atomic models are shown as stick models. Oxygen atoms are colored red, nitrogen blue, sulfur green, and carbon atoms according to the peptide chain (Pex7p, lime green; Pex21pC, light magenta; Fox3pN, yellow). Electron-density maps ($2F_o$-F_c density contoured at 1σ) are shown as meshes. Residues are labeled according to the peptide chain (Pex7p, black; Pex21pC, light magenta; Fox3pN, yellow).

Supplementary Figure 4

Single-molecule structures of Pex7p and Pex21pC.
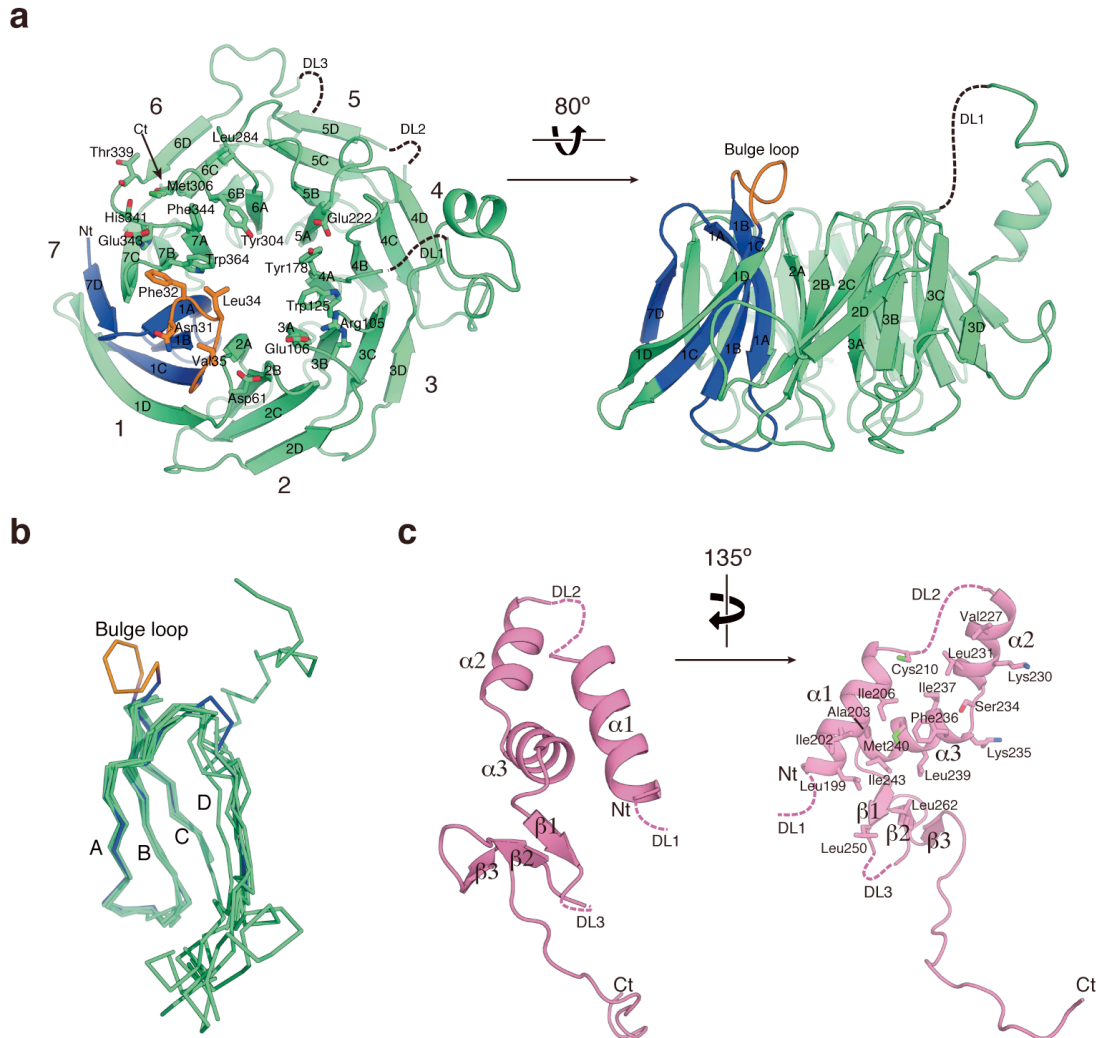
(a) Ribbon representation of Pex7p. The left molecule is in the same orientation as in Fig. 1c, right. (b) Structural alignment of the N-terminal 44 residues (blue and orange) of Pex7p with the other six WD40 motifs (lime green). The main chains are traced as sticks. (c) Ribbon representation of Pex21pC. The left molecule is in the same orientation as in Fig. 1c, right. Nt, N-terminus; Ct, C-terminus; DL, disordered loop.
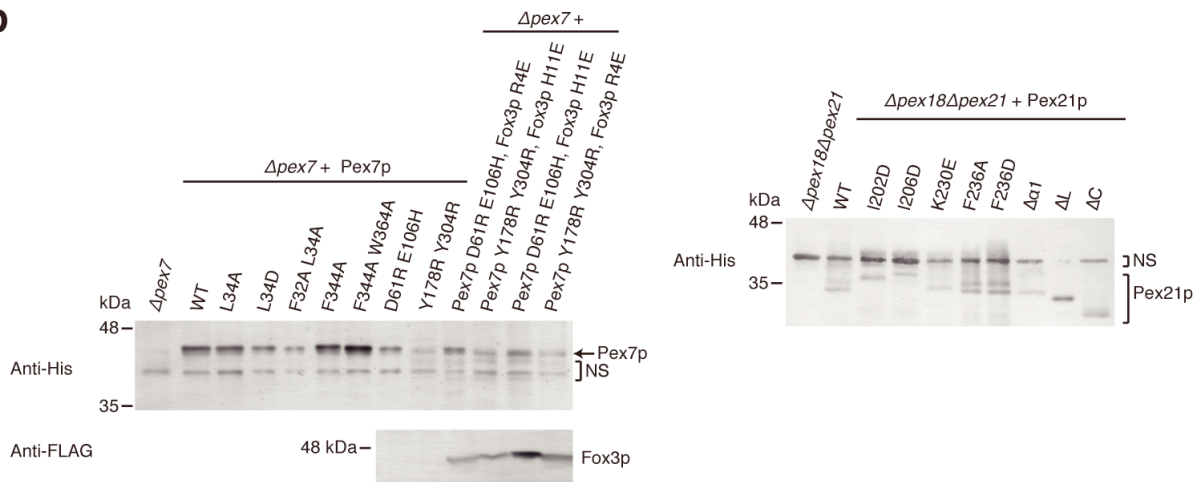
Supplementary Figure 5

In vivo Fox3pN-EGFP transport assays.

a
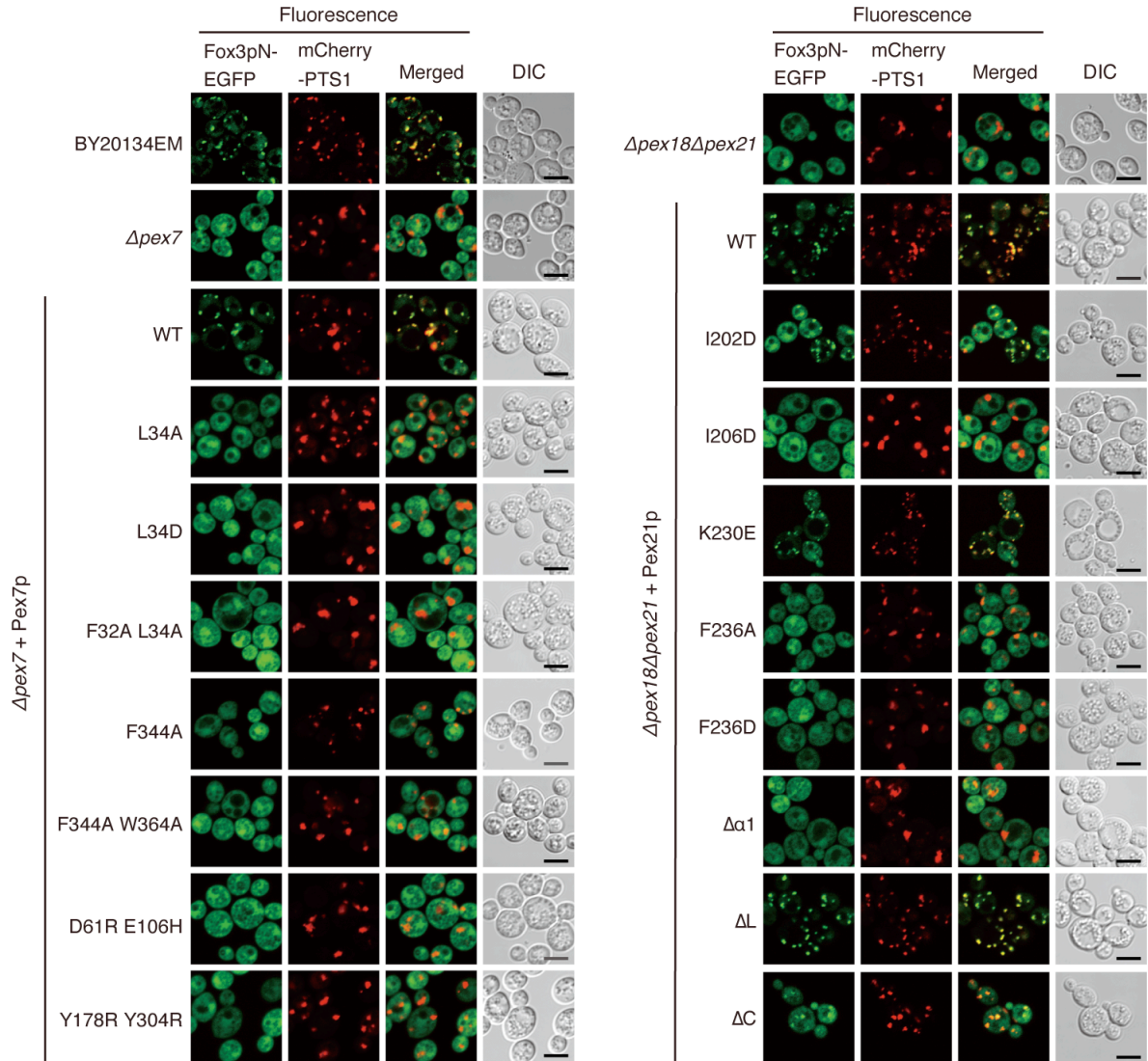
b

(a) The *S. cerevisiae* strains were grown in SCEO medium to an OD_{600} of 2, and live cells were examined with a confocal fluorescence microscopy. The intracellular localizations of Fox3pN-EGFP and mCherry-PTS1 were visualized by their fluorescence. The red spots of mCherry-PTS1 indicate the locations of peroxisomes, and the yellow spots in the merged fluorescence image indicate the co-localization of Fox3pN-EGFP and mCherry-PTS1. The scale bars in the differential interference contrast (DIC) images represent 5 μm. (b) The expression levels of Pex7p, Pex21p, and Fox3p variants were confirmed by western blotting. Pex7p and Pex21p variants contained His_6-tags at their C-termini, and were detected by western blotting using penta-His-specific HRP conjugate antibody. Fox3p variants contained FLAG-tags at their C-termini, and were detected using FLAG-specific antibody. NS indicates non-specific *S. cerevisiae* proteins, which bound to Ni-IMAC resin and were detected by the penta-His-specific HRP conjugate antibody. WT, wild type.

Supplementary Table 1

Plasmids used in this study.

Plasmid	Description	Source
pAG425GPD-ccdB-HA	*LEU2, 2μ, Amp^R*	Addgene
pAG426GPD-ccdB-HA	*URA3, 2μ, Amp^R*	Addgene
pAG304GPD-ccdB-EGFP	*TRP1, Amp^R*	Addgene
pAG303GPD-ccdB-HA	*HIS3, Amp^R*	Addgene
pmCherry	*Amp^R,* mCherry-tag	Clontech
pAG304-Fox3pN-EGFP/mCherry-PTS1	*FOX3 promoter driving FOX3N-EGFP, GPD promoter driving MCHERRY-SKL, TRP1, Amp^R*	This study
pAG425-Pex7p	*PEX7 promoter driving PEX7-His$_6$, LEU2, 2μ, Amp^R*	This study
pAG425-Pex7p(L34A)	*PEX7 promoter driving pex7(L34A)-His$_6$, LEU2, 2μ, Amp^R*	This study
pAG425-Pex7p(L34D)	*PEX7 promoter driving pex7(L34D)-His$_6$, LEU2, 2μ, Amp^R*	This study
pAG425-Pex7p(F32A L34A)	*PEX7 promoter driving pex7(F32A L34A)-His$_6$, LEU2, 2μ, Amp^R*	This study
pAG425-Pex7p(F344A)	*PEX7 promoter driving pex7(F344A)-His6, LEU2, 2μ, Amp^R*	This study
pAG425-Pex7p(F344A W364A)	*PEX7 promoter driving pex7(F344A W364A)-His$_6$, LEU2, 2μ, Amp^R*	This study
pAG425-Pex7p(D61R E106H)	*PEX7 promoter driving pex7(D61R E106H)-His$_6$, LEU2, 2μ, Amp^R*	This study
pAG425-Pex7p(Y178R Y304R)	*PEX7 promoter driving pex7(Y178R Y304R)-His$_6$, LEU2, 2μ, Amp^R*	This study
pAG303-Fox3p	*FOX3 promoter driving FOX3-FLAG, HIS3, Amp^R*	This study
pAG303-Fox3p(R4E)	*FOX3 promoter driving fox3(R4E)-FLAG, HIS3, Amp^R*	This study

pAG303-Fox3p(H11E)	*FOX3* promoter driving *fox3(H11E)-FLAG, HIS3, Amp^R*	This study
pAG426-Pex21p	*PEX21* promoter driving *PEX21-His$_6$, URA3, 2μ, Amp^R*	This study
pAG426-Pex21p(I202D)	*PEX21* promoter driving *pex21(I202D)-His$_6$, URA3, 2μ, Amp^R*	This study
pAG426-Pex21p(I206D)	*PEX21* promoter driving *pex21(I206D)-His$_6$, URA3, 2μ, Amp^R*	This study
pAG426-Pex21p(K230E)	*PEX21* promoter driving *pex21(K230E)-His$_6$, URA3, 2μ, Amp^R*	This study
pAG426-Pex21p(F236A)	*PEX21* promoter driving *pex21(F236A)-His$_6$, URA3, 2μ, Amp^R*	This study
pAG426-Pex21p(F236D)	*PEX21* promoter driving *pex21(F236D)-His$_6$, URA3, 2μ, Amp^R*	This study
pAG426-Pex21p(Δ197-211)	*PEX21* promoter driving *pex21(Δ197-211)-His$_6$, URA3, 2μ, Amp^R*	This study
pAG426-Pex21p(Δ214-229)	*PEX21* promoter driving *pex21(Δ214-229)-His$_6$, URA3, 2μ, Amp^R*	This study
pAG426-Pex21p(Δ247-288)	*PEX21* promoter driving *pex21(Δ247-288)-His$_6$, URA3, 2μ, Amp^R*	This study
pPICZA	*Zeocin^R*	Invitrogen
pGEX-6P-1	*Amp^R,* GST-tag, PreScission protease site	GE Healthcare
pMAL-c2E	*Amp^R,* MBP2-tag, Enterokinase site	NEB
pGEX6PT	*Amp^R,* GST-tag, PreScission protease site, TEV protease site	This study
pGEX6PT-Pex7p	*tac* promoter driving *GST-PEX7, Amp^R*	This study
pGEX6PT-Pex21pC	*tac* promoter driving *GST-PEX21C, Amp^R*	This study
pGEX6PT-Fox3p	*tac* promoter driving *GST-FOX3, Amp^R*	This study
pGEX6PT-Fox3pN-MBP	*tac* promoter driving *GST-FOX3N-MBP, Amp^R*	This study

pPICZA-GST-Pex7p	*AOX1* promoter driving *GST-PEX7, Zeocin^R*	This study
pPICZA-GST-Pex7p(Δ257-265)	*AOX1* promoter driving *GST-PEX7(Δ257-265), Zeocin^R*	This study
pPICZA-GST-Pex7p(F32A)	*AOX1* promoter driving *GST-PEX7(F32A), Zeocin^R*	This study
pPICZA-GST-Pex7p(L34A)	*AOX1* promoter driving *GST-PEX7(L34A), Zeocin^R*	This study
pPICZA-GST-Pex7p(L34D)	*AOX1* promoter driving *GST-PEX7(L34D), Zeocin^R*	This study
pPICZA-GST-Pex7p(F32A L34A)	*AOX1* promoter driving *GST-PEX7(F32A L34A), Zeocin^R*	This study
pPICZA-GST-Pex7p(F344A)	*AOX1* promoter driving *GST-PEX7(F344A), Zeocin^R*	This study
pPICZA-GST-Pex7p(F344A W364A)	*AOX1* promoter driving *GST-PEX7(F344A W364A), Zeocin^R*	This study
pMEXT-Pex21pC	*tac* promoter driving *MBP-PEX21C-His_6, Amp^R*	This study
pMEXT-Pex21pC(I202D)	*tac* promoter driving *MBP-PEX21C(I202D)-His_6, Amp^R*	This study
pMEXT-Pex21pC(I206D)	*tac* promoter driving *MBP-PEX21C(I206D)-His_6, Amp^R*	This study
pMEXT-Pex21pC(K230E)	*tac* promoter driving *MBP-PEX21C(K230E)-His_6, Amp^R*	This study
pMEXT-Pex21pC(F236A)	*tac* promoter driving *MBP-PEX21C(F236A)-His_6, Amp^R*	This study
pMEXT-Pex21pC(F236D)	*tac* promoter driving *MBP-PEX21C(F236D)-His_6, Amp^R*	This study
pMEXT-Pex21pC(Δ197-211)	*tac* promoter driving *MBP-PEX21C(Δ197-211)-His_6, Amp^R*	This study
pMEXT-Pex21pC(Δ214-229)	*tac* promoter driving *MBP-PEX21C(Δ214-229)-His_6, Amp^R*	This study
pMEXT-Pex21pC(Δ247-288)	*tac* promoter driving *MBP-PEX21C(Δ247-288)-His_6, Amp^R*	This study

Supplementary Table 2

Yeast strains used in this study.

S. cerevisiae Strain	Genotype	Source
BY20134 (W303-1A)	*MATa; ade2-1; can1-100; his3-11,15; leu2-3,112; trp1-1; ura3-1; rad5-535*	NBRP
BY20134EM	*MATa; ade2-1; can1-100; his3-11,15; leu2-3,112; trp1-1; ura3-1; rad5-535;* [pAG304-Fox3pN-EGFP/mCherry-PTS1]	This study
Δpex7	*MATa; ade2-1; can1-100; his3-11,15; leu2-3,112; trp1-1; ura3-1; rad5-535; pex7::URA3;* [pAG304-Fox3pN-EGFP/mCherry-PTS1]	This study
Δpex18Δpex21	*MATa; ade2-1; can1-100; his3-11,15; leu2-3,112; trp1-1; ura3-1; rad5-535; pex18::HIS3; pex21::LEU2;* [pAG304-Fox3pN-EGFP/mCherry-PTS1]	This study
Δpex7 + Pex7p WT	*MATa; ade2-1; can1-100; his3-11,15; leu2-3,112; trp1-1; ura3-1; rad5-535; pex7::URA3;* [pAG304-Fox3pN-EGFP/mCherry-PTS1], [pAG425-Pex7p)]	This study
Δpex7 + Pex7p L34A	*MATa; ade2-1; can1-100; his3-11,15; leu2-3,112; trp1-1; ura3-1; rad5-535; pex7::URA3;* [pAG304-Fox3pN-EGFP/mCherry-PTS1)], [pAG425-Pex7p(L34A)]	This study
Δpex7 + Pex7p L34D	*MATa; ade2-1; can1-100; his3-11,15; leu2-3,112; trp1-1; ura3-1; rad5-535; pex7::URA3;* [pAG304-Fox3pN-EGFP/mCherry-PTS1], [pAG425-Pex7p(L34D)]	This study
Δpex7 + Pex7p F32A L34A	*MATa; ade2-1; can1-100; his3-11,15; leu2-3,112; trp1-1; ura3-1; rad5-535; pex7::URA3;* [pAG304-Fox3pN-EGFP/mCherry-PTS1], [pAG425-Pex7p(F32A L34A)]	This study
Δpex7 + Pex7p F344A	*MATa; ade2-1; can1-100; his3-11,15; leu2-3,112; trp1-1; ura3-1; rad5-535; pex7::URA3;* [pAG304-Fox3pN-EGFP/mCherry-PTS1], [pAG425-Pex7p(F344A)]	This study

Δpex7 + Pex7p F344A W364A	*MATa; ade2-1; can1-100; his3-11,15; leu2-3,112; trp1-1; ura3-1; rad5-535; pex7::URA3;* [pAG304-Fox3pN-EGFP/mCherry-PTS1], [pAG425-Pex7p(F344A W364A)]	This study
Δpex7 + Pex7p D61R E106H	*MATa; ade2-1; can1-100; his3-11,15; leu2-3,112; trp1-1; ura3-1; rad5-535; pex7::URA3;* [pAG304-Fox3pN-EGFP/mCherry-PTS1], [pAG425-Pex7p(D61R E106H)]	This study
Δpex7 + Pex7p Y178R Y304R	*MATa; ade2-1; can1-100; his3-11,15; leu2-3,112; trp1-1; ura3-1; rad5-535; pex7::URA3;* [pAG304-Fox3pN-EGFP/mCherry-PTS1], [pAG425-Pex7p(Y178R Y304R)]	This study
Δpex7 + Pex7p D61R E106H, Fox3p R4E	*MATa; ade2-1; can1-100; his3-11,15; leu2-3,112; trp1-1; ura3-1; rad5-535; pex7::URA3;* [pAG304-Fox3pN-EGFP/mCherry-PTS1], [pAG425-Pex7p(D61R E106H)], [pAG303-Fox3p(R4E)]	This study
Δpex7 + Pex7p Y178R Y304R, Fox3p H11E	*MATa; ade2-1; can1-100; his3-11,15; leu2-3,112; trp1-1; ura3-1; rad5-535; pex7::URA3;* [pAG304-Fox3pN-EGFP/mCherry-PTS1], [pAG425-Pex7p(Y178R Y304R)], [pAG303-Fox3p(H11E)]	This study
Δpex7 + Pex7p D61R E106H, Fox3p H11E	*MATa; ade2-1; can1-100; his3-11,15; leu2-3,112; trp1-1; ura3-1; rad5-535; pex7::URA3;* [pAG304-Fox3pN-EGFP/mCherry-PTS1], [pAG425-Pex7p(D61R E106H)], [pAG303-Fox3p(H11E)]	This study
Δpex7 + Pex7p Y178R Y304R, Fox3p R4E	*MATa; ade2-1; can1-100; his3-11,15; leu2-3,112; trp1-1; ura3-1; rad5-535; pex7::URA3;* [pAG304-Fox3pN-EGFP/mCherry-PTS1], [pAG425-Pex7p(Y178R Y304R)], [pAG303-Fox3p(R4E)]	This study
Δpex18Δpex21 + Pex21p WT	*MATa; ade2-1; can1-100; his3-11,15; leu2-3,112; trp1-1; ura3-1; rad5-535; pex18::HIS3; pex21::LEU2;* [pAG304-Fox3pN-EGFP/mCherry-PTS1], [pAG426-Pex21p]	This study

Δpex18Δpex21 + Pex21p I202D	*MATa; ade2-1; can1-100; his3-11,15; leu2-3,112; trp1-1; ura3-1; rad5-535; pex18::HIS3; pex21::LEU2;* [pAG304-Fox3pN-EGFP/mCherry-PTS1], [pAG426-Pex21p(I202D)]	This study
Δpex18Δpex21 + Pex21p I206D	*MATa; ade2-1; can1-100; his3-11,15; leu2-3,112; trp1-1; ura3-1; rad5-535; pex18::HIS3; pex21::LEU2;* [pAG304-Fox3pN-EGFP/mCherry-PTS1], [pAG426-Pex21p(I206D)]	This study
Δpex18Δpex21 + Pex21p K230E	*MATa; ade2-1; can1-100; his3-11,15; leu2-3,112; trp1-1; ura3-1; rad5-535; pex18::HIS3; pex21::LEU2;* [pAG304-Fox3pN-EGFP/mCherry-PTS1], [pAG426-Pex21p(K230E)]	This study
Δpex18Δpex21 + Pex21p F236A	*MATa; ade2-1; can1-100; his3-11,15; leu2-3,112; trp1-1; ura3-1; rad5-535; pex18::HIS3; pex21::LEU2;* [pAG304-Fox3pN-EGFP/mCherry-PTS1], [pAG426-Pex21p(F236A)]	This study
Δpex18Δpex21 + Pex21p F236D	*MATa; ade2-1; can1-100; his3-11,15; leu2-3,112; trp1-1; ura3-1; rad5-535; pex18::HIS3; pex21::LEU2;* [pAG304-Fox3pN-EGFP/mCherry-PTS1], [pAG426-Pex21p(F236D)]	This study
Δpex18Δpex21 + Pex21p Δα1 (Δ197-211)	*MATa; ade2-1; can1-100; his3-11,15; leu2-3,112; trp1-1; ura3-1; rad5-535; pex18::HIS3; pex21::LEU2;* [pAG304-Fox3pN-EGFP/mCherry-PTS1], [pAG426-Pex21p(Δ197-211)]	This study
Δpex18Δpex21 + Pex21p ΔL (Δ214-229)	*MATa; ade2-1; can1-100; his3-11,15; leu2-3,112; trp1-1; ura3-1; rad5-535; pex18::HIS3; pex21::LEU2;* [pAG304-Fox3pN-EGFP/mCherry-PTS1], [pAG426-Pex21p(Δ214-229)]	This study
Δpex18Δpex21 + Pex21p ΔC (Δ247-288)	*MATa; ade2-1; can1-100; his3-11,15; leu2-3,112; trp1-1; ura3-1; rad5-535; pex18::HIS3; pex21::LEU2;* [pAG304-Fox3pN-EGFP/mCherry-PTS1], [pAG426-Pex21p(Δ247-288)]	This study

P. pastoris Strain	Genotype	Source
SMD1163	*his4; pep4; prb1*	Invitrogen
SMD1163 + GST-Pex7p	*his4; pep4; prb1;* [pPICZA-GST-Pex7p]	This study
SMD1163 + GST-Pex7p(Δ257-265)	*his4; pep4; prb1;* [pPICZA-GST-Pex7p(Δ257-265)]	This study
SMD1163 + GST-Pex7p(F32A)	*his4; pep4; prb1;* [pPICZA-GST-Pex7p(F32A)]	This study
SMD1163 + GST-Pex7p(L34A)	*his4; pep4; prb1;* [pPICZA-GST-Pex7p(L34A)]	This study
SMD1163 + GST-Pex7p(L34D)	*his4; pep4; prb1;* [pPICZA-GST-Pex7p(L34D)]	This study
SMD1163 + GST-Pex7p(F32A L34A)	*his4; pep4; prb1;* [pPICZA-GST-Pex7p(F32A L34A)]	This study
SMD1163 + GST-Pex7p(F344A)	*his4; pep4; prb1;* [pPICZA-GST-Pex7p(F344A)]	This study
SMD1163 + GST-Pex7p(F344A W364A)	*his4; pep4; prb1;* [pPICZA-GST-Pex7p(F344A W364A)]	This study

Supplementary Note

Plasmids

Escherichia coli expression plasmids for expression of Pex21pC, Fox3p, and Fox3pN-MBP as TEV-cleavable N-terminal GST-tagged proteins were constructed as follows. Expression vector pGEX6PT was created by modifying pGEX-6P-1 (GE Healthcare) by inserting a sequence (5'-GGATCTGGTACCGAAAACCTG TACTTCCAG-3') that encodes linker residues (Gly-Ser-Gly-Thr) and a TEV protease cleavage site (Glu-Asn-Leu-Tyr-Phe-Gln), immediately upstream of the *Bam*HI site of pGEX-6P-1. Coding sequences of *Saccharomyces cerevisiae* Pex21pC and Fox3p were amplified by PCR from yeast genomic DNA and inserted between the *Bam*HI and *Sal*I sites of pGEX6PT to obtain pGEX6PT-Pex21pC and pGEX6PT-Fox3p. Expression vector pGEX6PT-Fox3pN-MBP was constructed by replacing the coding sequence of Fox3p residues 16–417 of pGEX6PT-Fox3p with a linker (5'-AGATCC-3') followed by the coding sequence of *E. coli* MalE residues 27–396 (MBP), which was cloned from *E. coli* BL21(DE3) (Invitrogen) genomic DNA.

Pichia pastoris expression plasmids for expression of TEV-cleavable N-terminal GST-tagged Pex7p and its variants were constructed as follows. The coding sequence of *S. cerevisiae* Pex7p was amplified by PCR from *S. cerevisiae* genomic DNA and inserted between the *Bam*HI and *Sal*I sites of pGEX6PT. Next, the coding sequence of GST-Pex7p from pGEX6PT-Pex7p was subcloned into the pPICZA expression vector (Invitrogen) between the *Eco*RI and *Sal*I sites to yield pPICZA-GST-Pex7p. The plasmids for expression of Pex7p variants were created by site-directed mutagenesis of pPICZA-GST-Pex7p using a modified PCR method as described[5].

E. coli plasmids for expression of C-terminally His$_6$-tagged MBP-Pex21pC and its variants were constructed as follows. The plasmid pMEXT-Pex21pC was generated from pGEX6PT-Pex21pC by adding the coding sequence of the His$_6$-tag after the coding sequence of Pex21pC using an modified inverse PCR method[6] and exchanging the coding sequence of GST (5'-GTATTCATGTCCCCTATACT...TCCAGGGGCCCCTGGGATCT-3') for MBP

(5'-CATATGAAAACTGAAGAAGG...ACAATAACAACAACGGGCCC-3'), which was subcloned from pMAL-c2E (NEB). Deletions and point mutations were introduced to pMEXT-Pex21pC using site-directed mutagenesis as described above.

S. cerevisiae plasmid pAG425-Pex7p was constructed by amplifying the *PEX7* ORF plus 440 bp of upstream sequence from *S. cerevisiae* genomic DNA, inserting the resulting amplicon between the *Sac*I and *Hind*III sites of pAG425GPD-ccdB-HA[7] (Addgene), and replacing the coding sequence of the HA$_3$-tag (5'-ATGTACCCATACGATGTTCCTGACTATGCGGGCTATCCCTATGACGTCCCGG ACTATGCAGGATCCTATCCATATGACGTTCCAGATTACGCTGCTCAGTGC-3') with that of the His$_6$-tag (5'-CATCATCATCATCATCAT-3') by the inverse PCR method described above. Likewise, pAG426-Pex21p was constructed by amplifying the *PEX21* ORF plus 520 bp of upstream sequence, inserting this amplicon between the *Sac*I and *Hind*III sites of pAG426GPD-ccdB-HA[7] (Addgene), and replacing the coding sequence of the HA$_3$-tag with that of the His$_6$-tag. Expression of His$_6$-tagged Pex7p and Pex21p was regulated under control of their original promoters and the *CYC1* terminator. Plasmids expressing variants of Pex7p and Pex21p were generated by the site-directed mutagenesis described above.

S. cerevisiae integrating plasmid pAG303-Fox3p was constructed by amplifying the *FOX3* ORF plus 380 bp of upstream sequence from *S. cerevisiae* genomic DNA, inserting this amplicon between the *Sac*I and *Xho*I sites of pAG303GPD-ccdB-HA[7] (Addgene), and inserting the coding sequence of FLAG-tag (5'-GATTATAAAGATGAT GATGATAAG-3') after the coding sequence of Fox3p by the inverse PCR method described above. Plasmids expressing the variants of Fox3p were generated by the site-directed mutagenesis described above.

Bicistronic *S. cerevisiae* integrating plasmid pAG304-Fox3pN-EGFP/mCherry-PTS1 was constructed to enable simultaneous expression of Fox3pN-EGFP and mCherry-SKL. This plasmid was generated by replacing the DNA sequence between *Sac*I and *Kpn*I site of pAG304GPD-ccdB-EGFP[7] (Addgene) with tandem expression cassettes for Fox3pN-EGFP and mCherry-SKL. The coding sequence of Fox3pN-EGFP was placed

between the *S. cerevisiae FOX3* promoter (upstream 380-bp regulatory region of *FOX3*) and the *CYC1* terminator, and the coding sequence of mCherry-SKL was placed between *GPD* promoter and the *CYC1* terminator. The cDNA of mCherry was amplified from the pmCherry vector (Clontech).

All the constructs were verified by DNA sequencing before being used for protein expression. The list of all plasmids used in this study is presented in Supplementary Table 1.

Western blotting

S. cerevisiae cells (0.2 g) grown in SCEO medium (0.67% yeast nitrogen base with ammonium sulfate without amino acids, 2% (v/v) ethanol, 0.1% (w/v) oleic acid, 0.4% (w/v) Tween 40, appropriate amino acids, uracil, and adenine) to an OD_{600} of 2 were suspended in 300 μl buffer B (30 mM Tris-HCl pH 7.5, 300 mM NaCl, 1 mM DTT) containing 1 mM PMSF and lysed by vortexing with glass beads. Cleared lysate (350 μl) was supplemented with imidazole to a concentration of 20 mM and incubated with 15 μl Ni-IMAC resin for 1 h at 4°C. After washing the resin three times with 500 μl buffer B containing 20 mM imidazole, proteins were eluted with 20 μl buffer B containing 400 mM imidazole. C-terminally His_6-tagged Pex7p and Pex21p variants were detected by subjecting 5 μl eluted fraction to SDS-PAGE and western blotting using Penta-His HRP Conjugate (QIAGEN). C-terminally FLAG-tagged Fox3p variants were detected by subjecting cell lysate containing 30 μg protein to SDS-PAGE and western blotting using anti-FLAG antibody M2 (Sigma) and anti-mouse IgG HRP-linked antibody (GE Healthcare).

References for Supplementary materials

1. Thompson, J.D., Higgins, D.G. & Gibson, T.J. CLUSTAL W: improving the sensitivity of progressive multiple sequence alignment through sequence weighting, position-specific gap penalties and weight matrix choice. *Nucleic Acids Res.* **22**, 4673-4680 (1994).

2. Braverman, N. et al. Mutation analysis of PEX7 in 60 probands with rhizomelic chondrodysplasia punctata and functional correlations of genotype with phenotype. *Hum. Mutat.* **20**, 284-297 (2002).

3. Motley, A.M. et al. Mutational spectrum in the PEX7 gene and functional analysis of mutant alleles in 78 patients with rhizomelic chondrodysplasia punctata type 1. *Am. J. Hum. Genet.* **70**, 612-624 (2002).

4. Rehling, P. et al. The import receptor for the peroxisomal targeting signal 2 (PTS2) in Saccharomyces cerevisiae is encoded by the PAS7 gene. *EMBO J.* **15**, 2901-2913 (1996).

5. Sawano, A. & Miyawaki, A. Directed evolution of green fluorescent protein by a new versatile PCR strategy for site-directed and semi-random mutagenesis. *Nucleic Acids Res.* **28**, E78 (2000).

6. Erster, O. & Liscovitch, M. A modified inverse PCR procedure for insertion, deletion, or replacement of a DNA fragment in a target sequence and its application in the ligand interaction scan method for generation of ligand-regulated proteins. *Methods Mol. Biol.* **634**, 157-174 (2010).

7. Alberti, S., Gitler, A.D. & Lindquist, S. A suite of Gateway cloning vectors for high-throughput genetic analysis in Saccharomyces cerevisiae. *Yeast* **24**, 913-919 (2007).